3 Pacemaker Mechanisms Driving Pyeloureteric Peristalsis: Modulatory Role of Interstitial Cells

Richard J. Lang and Hikaru Hashitani

Abstract

The peristaltic pressure waves in the renal pelvis that propel urine expressed by the kidney into the ureter towards the bladder have long been considered to be 'myogenic', being little affected by blockers of nerve conduction or autonomic neurotransmission, but sustained by the intrinsic release of prostaglandins and sensory neurotransmitters. In uni-papilla mammals, the funnel-shaped renal pelvis consists of a lumen-forming urothelium and a stromal layer enveloped by a plexus of 'typical' smooth muscle cells (TSMCs), in multi-papillae kidneys a number of minor and major calyces fuse into a large renal pelvis. Electron microscopic, electrophysiological and Ca^{2+} imaging studies have established that the pacemaker cells driving pyeloureteric peristalsis are likely to be morphologically distinct 'atypical' smooth muscle cells (ASMCs) that fire Ca^{2+} transients and spontaneous transient depolarizations (STDs) which trigger propagating nifedipine-sensitive action potentials and Ca^{2+} waves in the TSMC layer. In unicalyceal kidneys, ASMCs predominately locate on the serosal surface of the proximal renal pelvis while in multi-papillae kidneys they locate within the sub-urothelial space. 'Fibroblast-like' interstitial cells (ICs) located in the sub-urothelial space or adventitia are a mixed population of cells, having regional and species-dependent expression of various Cl^-, K^+, Ca^{2+} and cationic channels. ICs display asynchronous Ca^{2+} transients that periodically synchronize into bursts that accelerate ASMC Ca^{2+} transient firing. This review presents current knowledge of the architecture of the proximal renal pelvis, the role Ca^{2+} plays in renal pelvis peristalsis and the mechanisms by which ICs may sustain/accelerate ASMC pacemaking.

Keywords

Pyeloureteric peristalsis · Atypical smooth muscle cells · Interstitial cells · Calcium imaging · Calcium channels · Pacemaking Upper urinary tract

Electronic Supplementary Material The online version of this chapter (https://doi.org/10.1007/978-981-13-5895-1_3) contains supplementary material, which is available to authorized users.

R. J. Lang (✉)
School of Biomedical Sciences, Faculty of Medicine, Nursing and Health Sciences, Monash University, Clayton, VIC, Australia
e-mail: rick.lang@monash.edu

H. Hashitani
Department of Cell Physiology, Graduate School of Medical Sciences, Nagoya City University, Nagoya, Japan
e-mail: hasitani@med.nagoya-cu.ac.jp

H. Hashitani, R. J. Lang (eds.), *Smooth Muscle Spontaneous Activity*, Advances in Experimental Medicine and Biology 1124, https://doi.org/10.1007/978-981-13-5895-1_3

3.1 Introduction

Kidneys are thought to have first evolved in freshwater bony fish. To maintain their body fluids at osmotic concentrations greater than their surrounds, freshwater fish, amphibians and reptiles actively transport salt into their blood via their gills or skin, while their kidneys produce a dilute urine. In contrast, marine fish and reptiles swallow seawater, actively eliminate salt across their gills or via facial salt glands and excrete an isotonic urine by reabsorbing salt and water in their kidneys. Only birds and mammals can excrete waste products in a hypertonic urine. Birds concentrate their urine twice their blood concentration, while human kidneys can concentrate urine about four times greater than blood plasma. The kidneys of desert mammals can excrete urine 10–20-fold more concentrated than their blood plasma. The kidneys of the kangaroo rat are so efficient, it obtains all the its water needs from its food and respiration [1].

The mammalian kidney is a complex organ consisting of up to a million filtrating units called nephrons. Blood pressure forces blood through the glomerulus capillary bed at the top of each nephron. The glomerulus retains the red blood cells, proteins and other large molecules, but allows water, small molecules and waste products to pass into the surrounding Bowman's capsule which empties into the proximal tubule of the nephron. Sugars, amino acids, and ions are recovered by active transport in the proximal tubule, while water and salts are reabsorbed in the lower Loops of Henle which extend deep into the renal medulla. The remaining fluid and metabolic wastes are secreted as urine.

3.2 Ultrastructure of the Upper Urinary Tract

In small mammals, urine produced by the nephron units within a single 'pyramid-shaped' inner-medulla/papilla complex is secreted into a funnel-shaped renal pelvis which has a number of radiating 'finger-like' spokes for attachment to the kidney parenchyma (Fig. 3.1a). Between these spokes the outer margin of the pelvis forms a concave-shaped edge creating secondary pouches between the pelvis and the kidney parenchyma. In sections of kidney, this region between spokes appears as a thick 'bulb' ending of the pelvis wall, while the spokes appear as long gradually thinning tapers [2, 3]. To cope with the filtering of relatively large volumes of blood, some larger mammals have evolved compound (humans, sheep and pigs) or discrete (whales and seals) multi-papillae kidneys, so that urine is expressed by a number of papillae into minor calyces similar in appearance to a single-papilla renal pelvis. These minor calyces fuse into several major calyxes which fuse into a single renal pelvis that extends to the ureter.

In single-papilla kidneys, the renal pelvic wall consists of a lumen-forming squamous urothelium, basal epithelial cells (BECs) and a thin layer of stromal cells enveloped by a plexus of 'typical' smooth muscle cell (TSMC) bundles. The BECs facing the proximal inner medulla are squamous or low cuboidal in shape, contain a large round nucleus, numerous dense bodies, mitochondria and free ribosomes and long interconnecting projections to form a continuous layer of cells [3, 4] (Fig. 3.1c, Supplementary Video 3.1). BECs occupy the same morphological space as cells that are intensely immunoreactive to antibodies raised against the $K_V7.5$ (KCNQ5) channel subunit [3, 5]. TMSCs, intensely immunoreactive to antibodies raised against α-smooth muscle actin (α-SMA), also form a continuous layer of circumferentially orientated bundles of densely packed cells adjacent to the urothelium originating near the base of the papilla and extending into the ureter [6–8]. $K_V7.5^+$ BECs and TSMCs both increase in number and density with distance from the base of the papilla so in regions distal of the fornix the renal pelvis consists of a thick tightly packed transitional epithelial layer enveloped by a thick TSMC coat.

An additional layer of lightly α-SMA$^+$ obliquely oriented 'atypical' smooth muscle cells (ASMCs) locates on the *serosal* surface of the renal pelvis wall of single-papilla kidneys. These ASMCs are not arranged in bundles, but form a

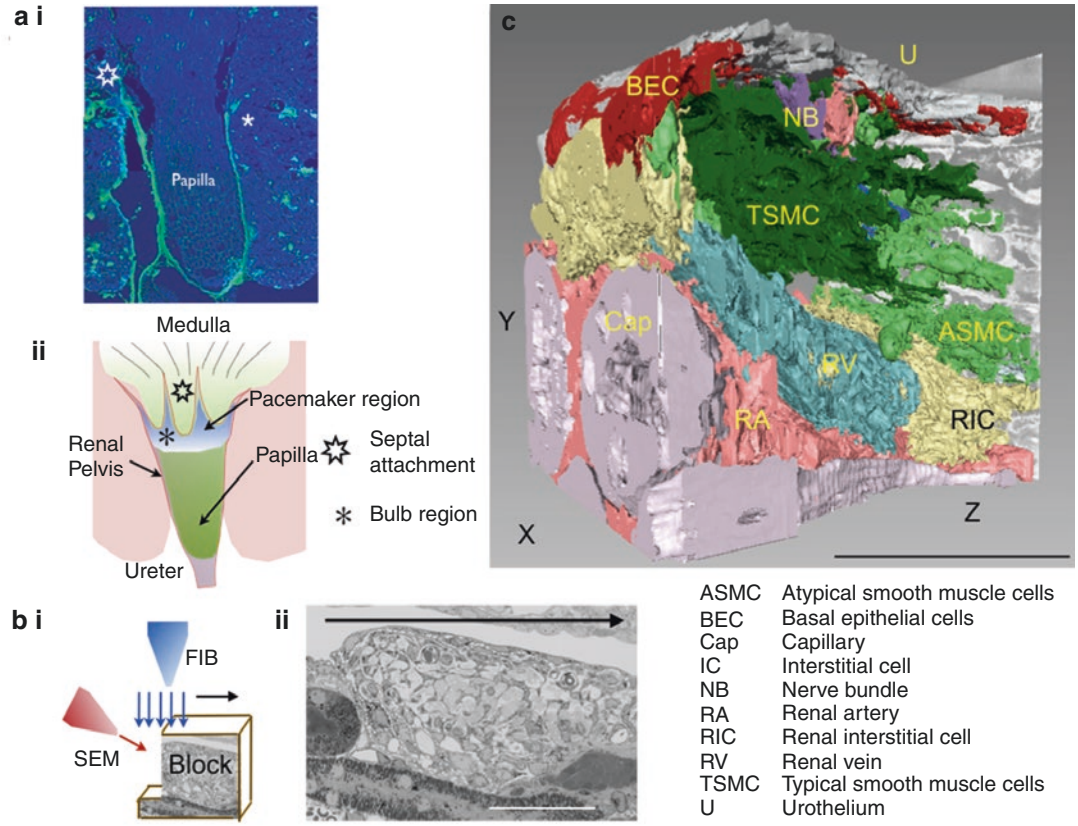

Fig. 3.1 The architecture of the 'bulb' region of mouse proximal renal pelvis examined using FIBSEM tomography. (**ai**) Single caudal section the mouse renal pelvis illustrating that the funnel-shaped muscle wall (**ai** *green*, **aii**) either forms 'spoke-like' attachments (*star*) to the kidney parenchyma or ends abruptly as a 'bulb' (*). (**bi**) Schematic of the focused ion beam scanning electron microscope (FIBSEM) in which the X–Y surface of a block of the bulb region of the renal pelvis is repeatedly milled in the Z direction (**bii** *arrow*) using the FIB, each new X–Y surface is then imaged using the SEM. (**c**) Similar-looking cells and structures within the block of 900 ortho-slice micrographs were identified, volume rendered and colour coded for easy identification. Calibration bars: 50 μm (**bii**), 0.5e^5 nm (**c**). Figure from Hashitani et al. [3]

thin sheet of loosely arranged groups of cells separated by a network of collagen connective tissue. In multi-papillae kidneys, ASMCs form a thin *inner* layer between the urothelial and TSMC layers of each minor calyx [9, 10]. These ASMCs extend over the renal parenchyma and fuse with the TSMC layer to form a continuous layer between minor calyces. In both single-papilla and multi-papillae kidneys, the ASMC layer does not extend past the pelviureteric junction into the ureter [6, 8–11].

When viewed with a standard electron microscope, TSMCs in single slices display a round darkly stained cytoplasm due to the abundance of numerous longitudinally arranged myofilaments and a large oval-shaped nucleus. In contrast, ASMCs are lightly stained due to their sparsely distributed myofilaments separated by large areas of clear cytoplasm containing small mitochondria, granular endoplasmic reticulum and Golgi cisternae [2, 6, 8, 10]. In single light or electron micrographs, ASMCs appear to have a rounded nuclear region with a number of radiating thin projections and have previously been interpreted as being 'stellate' or 'spindle shaped' (Fig. 3.2ai) [6, 8, 12, 13]. The repeated milling of a block of mouse renal pelvis and imaging of each new surface using focused ion beam scanning electron

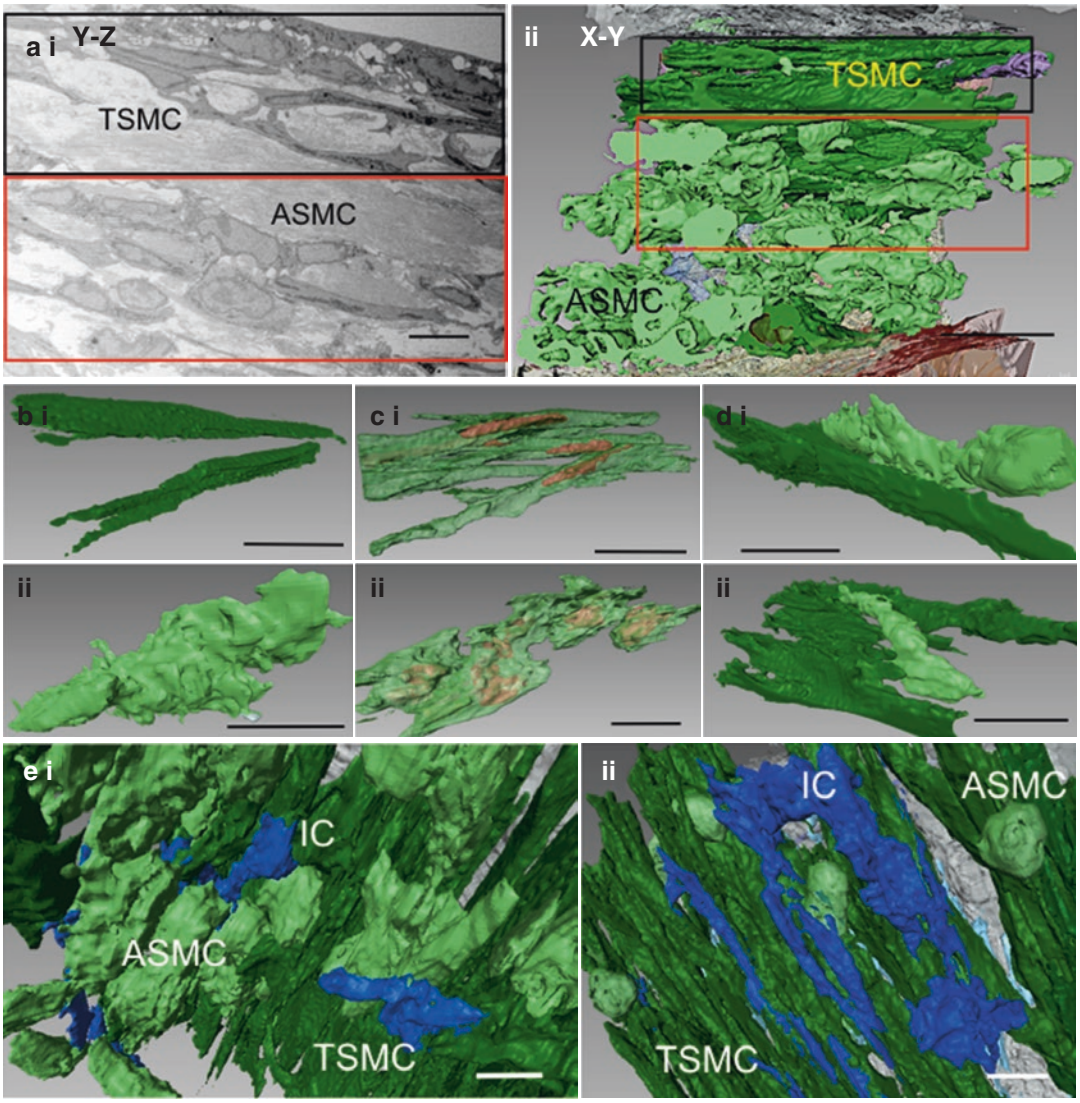

Fig. 3.2 Single cell reconstructions and close appositions of ASMCs, TSMCs and ICs in the mouse renal pelvis. (**ai**) Example of a single X–Y electron micrograph within a stack of ortho-slices illustrating the morphological difference between ASMCs (**ai** *red square*) and TSMCs (**ai** *black square*). (**aii**) Volume rendering all of the cells within the same region reveals the structure and regions occupied by TSMCs (*dark green*) and ASMCs (*light green*) present. Typical examples of single or groups of TSMCs (**bi**, **ci**) and ASMCs (**bii**, **cii**) and their close apposition with like cells, projected as being solid (**bi**, **ii**) or relatively transparent (**ci**, **ii**) to reveal their volume-rendered nuclei. (**di**, **ii**) Examples of close appositions of TSMCs and ASMCs in the proximal renal pelvis. (**e**) Micrographs of volume-rendered TSMCs, ASMCs and serosal ICs (*dark blue cells*), in the bulb (**ei**) and mid region (**eii**) of the renal pelvis to illustrate their architecture and close appositions. Calibration bars: 0.5 μm (**a**), $0.3e^4$ nm (**bi**), $2e^5$ nm (**bii**), $1e^4$ nm (**ci**, **ii**, **di**), $0.2e^4$ nm (**dii**), $2e^{13}$ nm (**e**). Figure adapted from Hashitani et al. [3]

microscope (FIB SEM) tomography (Fig. 3.1) have established that volume-rendered TSMCs are long cigar-shaped 'spindles' (Fig. 3.2bi). In addition, the thin ASMC projections are in fact continuous, resembling the rim of an irregular saucer or a leaf [3] (Fig. 3.2bii) and forming close appositions with neighbouring ASMCs and TSMCs (Fig. 3.2c, d) [3, 6, 8–10, 12, 13]. In the

spoke attachments, ASMCs are loosely arranged in a basket weave arrangement while in the bulb region they are mostly orientated in the longitudinal direction [3] (Supplementary Video 3.1). In contrast, TSMC are mostly absent as the spoke attachments approach the parenchymal tissue [2, 3, 5, 8, 13].

As ASMCs are sparsely endowed with contractile filaments and the relative number of ASMCs, compared to TSMCs, decreases with distance from the inner medulla to the ureteropelvic junction in both single- and multi-papillae kidneys [8, 10], Dixon and Gosling proposed that ASMCs might have a function different from contractile TSMCs, that they may be the pacemaker cells driving the movement of urine towards the bladder [6, 9, 10, 12].

3.3 Pyeloureteric Peristalsis

The upper urinary system has evolved to transport urine from the kidney to the bladder as the absence of an active drainage would lead to the development of back pressure-induced damage and fibrosis within the inner medulla and kidney parenchyma. This movement of urine occurs by the means of spontaneous propagating peristaltic contractions (pyeloureteric peristalsis). From the earliest investigations into pyeloureteric peristalsis [14], it has been recognized that the upper urinary tract exists as a syncytium and that the excitation originates in the proximal renal pelvis and travels distally towards the bladder [15–20]. As the papilla and inner medulla are not contractile, the hydrostatic pressure changes that occur during these peristaltic contractions may also have a 'milking' action to promote the secretion of urine [7, 21]. The myogenic nature of pyeloureteric peristalsis is also demonstrated by the presence of spontaneous contractions in vivo after denervation, or ex vivo after nerve conduction blockade [15, 22–24].

Propagating contractions and associated pressure waves in the renal pelvis and ureter are preceded by an electrical impulse [16, 17, 25–28] that is initiated at the pelvi-papilla border [19, 20, 29]. Early extracellular recordings from the porcine multi-papillae kidney suggested that minor calyces can discharge synchronously or asynchronously [30] and that the calyx firing at the highest frequency drives the pelvic contractions. The excitation frequencies of the major calyces, renal pelvis and ureter are multiples of the discharge frequency within the dominate minor calyx [31–33], thus creating a decreasing frequency gradient down the upper urinary system [27, 34–36]. Recordings in the multi-papillae sheep kidney [37] using multiple-mapping electrodes have demonstrated that excitation originates in only one minor calyx to drive the wave of excitation into the renal pelvis and that this site of initiation moves spontaneously between calyces. If two sites of excitation discharge near simultaneously, one site predominates, sometimes alternatively, blocking the conduction of the wave of excitation from the other site. Complete or partial conduction block of the waves of excitation within the renal pelvis can also occur anywhere, anytime [37].

Rodent uni-papilla kidneys display a similar single origin of the wave of excitation in the most proximal regions of the pelvi-papilla border [38, 39] that will dominate lesser sites of excitation and which can spontaneously shift along the border. Spontaneous contractions can also randomly originate in the mid and distal renal pelvis [22, 40]. In the rat renal pelvis, the peristaltic wave travels from the pelvi-papilla border to the mid renal pelvis and often triggers a number of additional high frequency contractions that can travel in both antegrade and retrograde directions [2, 23, 41]. When the pacemaker drive from the proximal region of uni-papilla or multi-papillae kidneys is prevented upon transection [22, 42, 43] or upon pharmacological blockade of hyperpolarization-activated cation nucleotide gated (HCN) channels [38, 39], the more distal regions readily trigger waves of excitation.

Circumferentially oriented strips cut from the uni-papilla renal pelvis [44–46] or from the minor and major calyces and renal pelvis of multi-papillae kidney [47] contract spontaneously in vitro at the same frequency when they are obtained from the same distance from the inner medulla pelvis border. However, their

contraction frequency decreases as they are cut from regions increasingly more distal of the inner medulla/papilla complex(es) [18, 36, 45–48]. Stretch of strips of renal pelvis and ureter increases contractile force to an optimal maximum muscle length, beyond which muscle force decreases [22, 49]. This stretch-induced increase in muscle tone in human and sheep renal pelvic strips is associated with an increase in contraction frequency [50], but not in strips from the rabbit [51] or guinea pig [15, 22] renal pelvis. However, urine volume or wall stretch appears to increase the likelihood of a one-to-one propagation of excitation from the renal pelvis into the ureter [32, 52].

The *decreasing* frequency of the spontaneous contractions in strips from uni-papilla renal pelvis and the minor and major calyces and renal pelvis of multi-papillae kidneys contraction with distance from the inner medulla/papilla complex(es) [6, 8–10, 12] has been suggested to arise from the *decreasing* number of 'pacemaker' ASMCs [6, 44] and with the *increasing* number of TSMCs expressing 'refractory' K^+ membrane conductances [8, 53]. Alternatively, these data have led to the concept of *'latent' pacemakers* [20], which some suggest arise from the pacemaker activity of intrinsic interstitial cells (ICs).

3.4 Sub-urothelial and Serosal ICs

Light and electron microscopy has established that 'fibroblast-like' ICs in the rodent renal pelvis are sparsely distributed in both the adventitia and sub-urothelial space, separated by regions of dense bundles of collagen [8, 13]; the absence of any fibronexus indicating that they are not myofibroblasts. These ICs display numerous caveolae, an incomplete basal lamina and many other morphological characteristics used previously to distinguish interstitial cells of Cajal (ICC) in the gastrointestinal tract [8]. Volume rendering of ICs imaged in serial sections of mouse renal pelvis using FIBSEM tomography reveals that they are in fact 'ribbon shaped', that they make close appositions with like cells, as well as neighbouring ASMCs and TSMCs (Fig. 3.2e), and that they *increase* in number with distance from the papilla base [3, 8] (see Supplementary Video 3.1).

Immunohistochemical analysis of the mouse renal pelvis has established that ICs represent a mixed population of cells that has yet to be fully characterized. Like ICC, some α-SMA$^-$ ICs are intensely immuno-positive for antibodies against the Ca^{2+}-activated Cl^- channel protein Ano1 and mildly immuno-positive for $K_V7.5$ antibodies [2, 5]. These α-SMA$^-$ Ano1$^+$ $K_V7.5^+$ ICs are likely to be the freshly isolated ICs that display spontaneous niflumic acid-sensitive transient Cl^- currents, as well as voltage-dependent K^+ current sensitive to the $K_V7.x$ channel blocker XE911 when recorded using patch clamp technology [5]. These Ano1$^+$ $K_V7.5^+$ ICs do not appear to have the same distribution as α-SMA$^-$ intensely PDGFRα-eGFP$^+$ ICs in the lamina propria and serosa of the renal pelvis of B6.129S4-Pdgfrα$^{tm11(EGFP)sor}$/J mice [3]. Interestingly, the nuclei of serosal ASMCs displaying spontaneous Ca^{2+} transients also lightly express PDGFRα-eGFP fluorescence (H Hasitani & RJ Lang unpublished observations), suggesting that PDGFRα-eGFP$^+$ cells in the mouse real pelvis are not a homocellular population.

3.4.1 $Ca_V3.x^+$ HCN3$^+$ ICs

In coronal sections of the mouse renal pelvis, ICs immunoreactive to antibodies against T-type voltage-dependent Ca^{2+} channel (TVDCC) $Ca_V3.1$ ($Ca_V3.1^+$) are selectively located in the same proximal regions as ICs that are also immunoreactive to antibodies raised against HCN isoform 3 channel subunits (HCN3$^+$) [3]. Indeed, HCN3 staining has been co-located with $Ca_V3.1$ channel immunoreactivity in the mouse renal pelvis [39] and $Ca_V3.2$ channel immunoreactivity in porcine and human multi-papillae kidneys [54]. There appears to be some confusion as to whether $Ca_V3.1$ or HCN3 staining also co-locates with α-SMA immunoreactivity. HCN3$^+$ cells have been reported to be 'integrated' within the smooth muscle layer of the proximal region of the mouse renal pelvis [38, 39] and the minor calyces of porcine and human kidney [54]. In our hands, $Ca_V3.1^+$ ICs are clearly not α-SMA positive and lay only in the sub-urothelial

space of the proximal renal pelvis [3]. In contrast, Hurtado et al. reported that HCN3$^+$ $Ca_V3.1^+$ cells are also α-SMA$^+$ [38]. In the minor calyces of the porcine kidney, HCN3$^+$ cells display both α-SMA and $Ca_V3.2$ immunoreactivity, while HCN3$^+$ $Ca_V3.2^+$ cells in the human minor calyces don't co-locate with α-SMA immunoreactivity [54]. In spite of pharmacological evidence of the effects of the likely presence and blockade of $Ca_V3.2$ channels on Ca^{2+} signalling and contractility of the mouse renal pelvis [3], we and others [38, 39] have yet to demonstrate the presence of $Ca_V3.2$ channel immunoreactive product. Thus, the results obtained to date using presently available antibodies and methodologies appear to have some selectivity issues that have yet to be resolved.

3.4.2 Kit Staining in the Upper Urinary Tract

A number of researchers have reported the presence of spindle-shaped ICs in *sectioned* material of various regions of the ovine, rat [55], porcine [56], human [57, 58], mouse [59, 60] upper urinary tract that are immunoreactive to antibodies raised against the tyrosine kinase receptor Kit, the selective marker of ICC. In the mouse renal pelvis, this Kit$^+$ staining is found predominately in the serosal adventitia and less often in the muscle, sub-urothelial layers and urothelium [59, 60]. The intensity of this Kit staining also *decreases* slightly with distance from the papilla border [55, 57]. This Kit staining does not co-locate with markers for endothelial and epithelial cells, macrophages, hemopoietic/progenitor stem cells or mast cells [55, 57, 61]. When not tested immunohistologically, Kit$^+$ mast cells are readily identified by their distinctive circular shape [8, 62].

In the guinea pig renal pelvis, fibroblast-like ICs are readily identified using standard electron microscopy, while Kit antibodies only stain mast cells [8]. Recently, we have demonstrated that Kit (CD117 or AK2) staining in *whole mount* or *sectioned* preparations of mouse renal pelvis readily co-locates with the neuronal marker PGP9.5 [2, 5]. Thus, we have suggested that Kit staining of neurons in low-resolution light micrographs of *sectioned* material may well appear as 'spindle-shaped' Kit$^+$ cells. Kit staining of sectioned neural tracts may also explain the appearance of Kit staining during the functional development of the mouse upper urinary tract [60, 63] and its loss with obstruction [62, 64, 65] (see Sect. 3.9). A more rigorous examination of whether Kit and neuronal markers co-localize [55, 56] is required in both normal and pathological samples of the upper urinary tract, as well as animals that display a fluorescent reporter protein in cells that exclusively express Kit (e.g. Kit$^{+/copGFP}$ mice) [66].

3.5 Spontaneous Activity in the Upper Urinary Tract

3.5.1 Typical Smooth Muscle Cells

Early extracellular electrode [16, 17, 25–28], sucrose gap [36, 67–69] and intracellular microelectrode [8, 53, 70–75] recordings established that the upper urinary tract display spontaneous electrical activity and that migrating contractions associate with action potentials consisting of an initial rapidly-rising spike and a long plateau (Fig. 3.3ai, aii) [67, 68, 76–78], which in the guinea pig also triggers a number of additional high frequency spikes [8, 71, 73, 79, 80]. These action potentials that propagate down the renal pelvis (Fig. 3.3ci, cii) into the ureter are associated with a propagating Ca^{2+} wave within long spindle-shaped TSMCs (Fig. 3.4ai) [8] and it's this rise in Ca^{2+} that underlies the propagating contractions [77, 78, 81]. When viewed at higher magnifications, TSMC Ca^{2+} transients occur almost simultaneously along the length of each cell, while the wave propagates between cells in a direction perpendicular to their long axis (Fig. 3.4aii, b) [77], resulting in near simultaneous action potential discharge and contraction in the transverse axis of the renal pelvis and a slow propagation (at a velocity of 1.5–2 mm·s^{-1}) of excitation in the longitudinal axis (Fig. 3.4b) [77, 82, 83].

The action potentials and contractions in the mouse and guinea pig renal pelvis are dose-dependently reduced then abolished by the L-type voltage-dependent Ca^{2+} channel (LVDCC) blocker, nifedipine (1–10 μM) [73, 77, 78, 84] in a manner associated with a

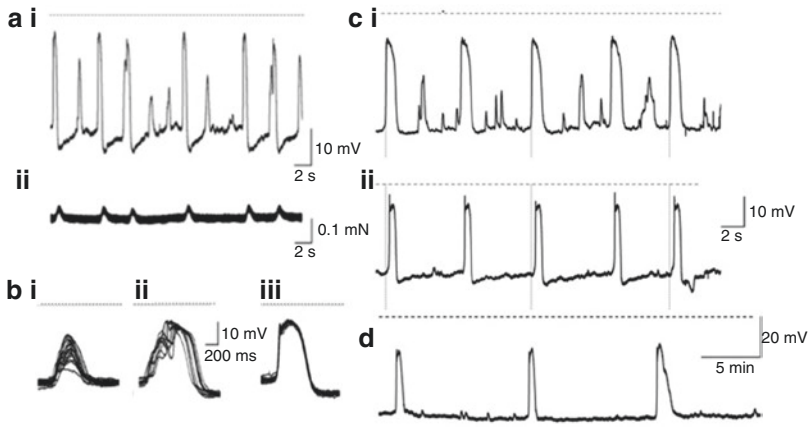

Fig. 3.3 Electrical recordings in the mouse renal pelvis. (**a**) Simultaneous recording of electrical (**ai**) and contractile (**aii**) activity illustrating that only action potentials and not STDS are associated with muscle contraction. (**b**) Recordings of superimposed STDs in the presence (**bi**) and absence (**bii**) of 1 μM nifedipine, illustrating their variable summation (**bi**) and triggering (**bii**) of an action potential. (**biii**) Superimposed action potentials to illustrate their time course. (**ci**, **ii**) Simultaneous recordings from two intracellular microelectrodes 240 μm apart illustrating that only action potentials propagate. (**d**) Recording of IC action potentials in the distal renal pelvis bathed in 1 μM nifedipine containing physiological salt solution, note the large difference in time scale

membrane depolarization of some 5–10 mV [79]. In the mouse renal pelvis, LVDCC blockade (1–3 μM nifedipine) reduces TSMC Ca^{2+} waves (Fig. 3.4ci, cii) and contraction amplitude [3], while blockade of TVDCCs (with Ml218, mibefradil, NNC55-0396 or R(-)efonidipine) reduces contraction frequency [3, 39]. The blockade of $Ca_V3.2$ channels with low concentrations (10 μM) of Ni^{2+} [85] also reduces contraction frequency without affecting their amplitude [3]. Higher concentrations of Ni^{2+} (100–300 μM) evoke a transient acceleration of TSMC Ca^{2+} activity associated with a transient rise in the basal Ca^{2+}, followed by gradual reduction in contraction frequency [3]. Blockade of both LVDCCs and TVDCCs (with 1–3 μM nifedipine and 10–100 μM Ni^{2+}) is necessary to completely arrest contractile activity and its underlying TSMC Ca^{2+} transients in the mouse renal pelvis [3].

3.5.2 Atypical Smooth Muscle Cells

Intracellular microelectrodes impalements of the renal pelvis of the mouse, guinea pig and rat reveal that spontaneous transient depolarizations (STDs) of a simple waveform and varying amplitude [74, 79, 86] are recorded in spindle-shaped ASMCs (Fig. 3.3ai, bi, and ci) [8, 23, 77]. These STDs are recorded most often in the 'spoke-like' attachments and bulb regions of the proximal renal pelvis [3, 8, 87]. Their likelihood of being recorded and their frequency of discharge also decreases with distance from the pelvis papilla border (Fig. 3.3c), they have never been recorded in the ureter [8, 87]. STDs, firing at a high frequency (5–30 min^{-1}) are often (Fig. 3.3ai, ci) but not always present between the spontaneous TSMC action potentials (5–12 min^{-1}), are not associated with muscle contraction (Fig. 3.3ai) and are little affected by the LDVCC- and TDVCC-independent Ca^{2+} entry blockers (Fig. 3.3ai), La^{3+} (or Gd^{3+}) [78] which blocks Ca^{2+} signalling in the rabbit urethra [88].

In the nifedipine (1 μM)-arrested mouse renal pelvis loaded with Ca^{2+} fluorophores fluo-4 or Cal 520, high frequency but slowly propagating intercellular Ca^{2+} waves are recorded in short cells at the same frequency as STDs and in the same adventitial region [77, 78] as ASMCs identified with standard electron microscopy or FIBSEM tomography [3] (see Supplementary

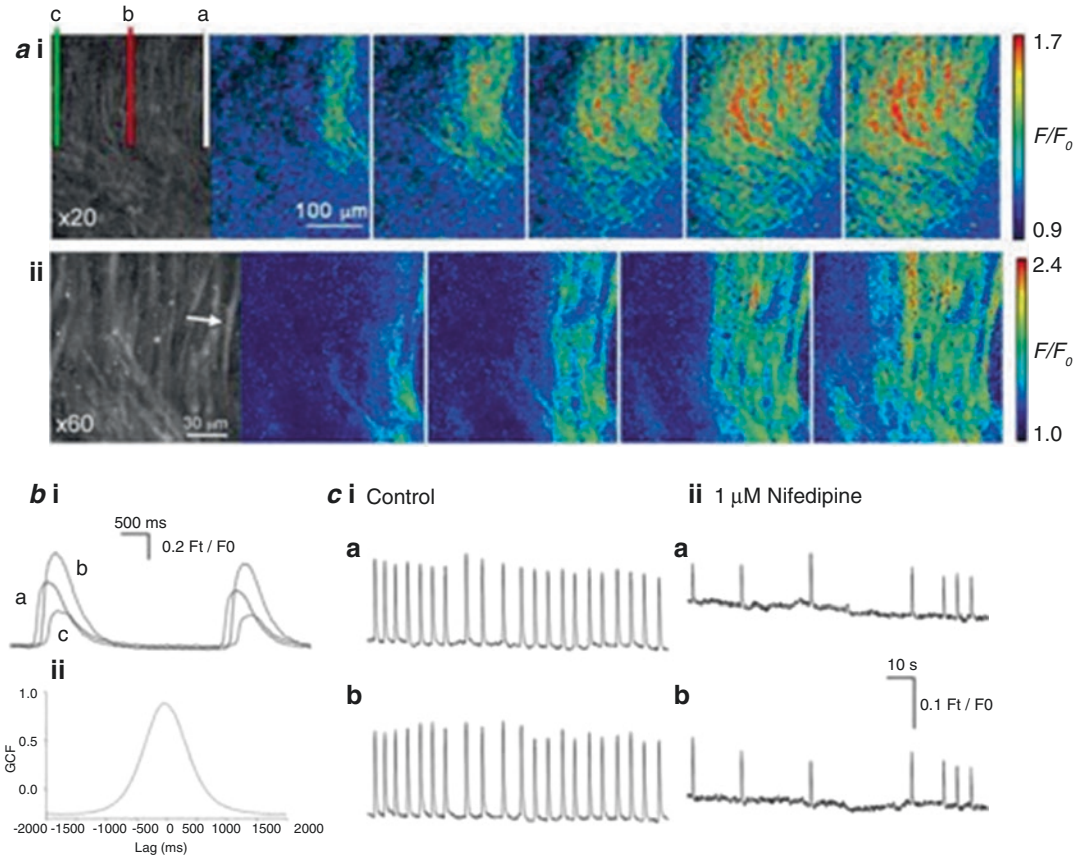

Fig. 3.4 Ca^{2+} waves in typical smooth muscle cells (TSMCs) of the renal pelvis **a** sequential Ca^{2+} fluorescence intensity micrographs of a fluo-4 loaded TSMC layer (time intervals of 66 ms at ×20 (**ai**) or ×60 (**aii**) magnification). The Ca^{2+} wave is clearly seen as a transient increase in Ca^{2+} intensity propagating across the field of view; the arrow indicates a single TSMC. (**bi**) Superimposed fluorescence intensities of the three regions (a–c) in **ai** plotted against time. (**bii**) Correlation of the Ca^{2+} waves recorded at a and c (separation 110 µm) show a high degree of 1:1 synchronicity. (**c**) Ca^{2+} waves recorded at two positions in a field of view (**ci**) were reduced but not completely blocked in 1 µM nifedipine (**cii**). Figure taken from Lang et al. [77]

Video 3.2). These ASMC Ca^{2+} transients sometimes propagate into neighbouring similar-shaped cells if located on their longitudinal axis and are only reduced, not blocked by 3–10 µM nifedipine. When bathed in 1 µM nifedipine and 100 µM Ni^{2+} the parameters (amplitude, frequency ½ width and integral) describing the time course of these ASMC Ca^{2+} transients are fitted by single Gaussian distributions (Fig. 3.5bi–biv) suggesting a single population of cells. ASMC Ca^{2+} transients are mostly asynchronous but appear to burst synchronously every 3–5 min. During these bursts the ASMC basal Ca^{2+} rises, the frequency of these ASMC Ca^{2+} signals doubles, while their other parameters are little affected (Fig. 3.5aiii) [3].

Contraction and action potential discharge in the guinea pig renal pelvis [82] and the firing of STDs and ASMC Ca^{2+} transients in the mouse renal pelvis [78] are dependent on the influx of external Ca^{2+}, sarcoplasmic endoplasmic reticulum Ca^{2+}-ATPase (SERCA)-dependent uptake of Ca^{2+} into internal stores, IP_3-dependent release from these endoplasmic reticulum stores and the cyclic movement of Ca^{2+} through mitochondria [89]. Contraction amplitude and frequency in the guinea pig renal pelvis [82] are little affected by 30 µM ryanodine, the blocker of ryanodine-

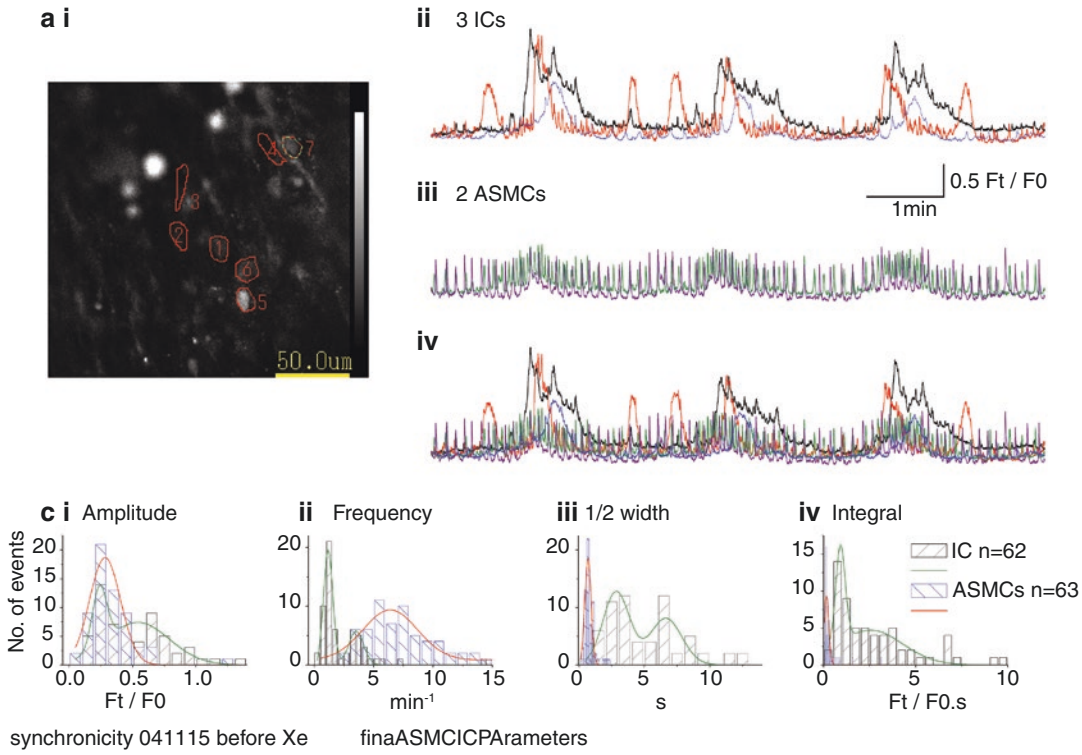

Fig. 3.5 Comparison of spontaneous Ca^{2+} transients in ICs and ASMCs in the mouse renal pelvis. (**ai**) Typical field of view of cells bathed in 1 μM nifedipine: 100 μM Ni^{2+}-containing physiological salt solution. Ca^{2+} transient activity (F_t/F_0) in three ICs (**ai** region of interest (ROIs) 1,2,5, **aii**) and two ASMCs (**ai** ROIs 3,4, **aiii**) plotted against time separately (**aii**, **iii**) and together (**aiv**). (**bi–iv**) Frequency distributions of four measured parameters of 63 ICs (*blue columns*) and 62 ASMCs (*black columns*) recorded *between* bursts were fitted (by least squares) with 1 (**b** *red* line ASMC) or 2 (**b** *green line* ICs) Gaussian distributions. ICs display spontaneous low frequency Ca^{2+} transients that synchronize into bursts every 3–5 min. Neighbouring ASMCs displaying higher-frequency spontaneous Ca^{2+} transients, also accelerate their firing in synchrony with the bursting ICs. Figure adapted from Hashitani et al. [3]

sensitive Ca^{2+} release channels. The amplitude, ½ width and synchronization of STDs in the mouse renal pelvis are also reduced by ryanodine (30–100 μM) which reduces their ability to sum into a depolarization sufficiently large to trigger an TSMC action potential [78]. However, ryanodine (100 μM) has little effect on any ASMC Ca^{2+} transient parameters [78]. These minor inhibitory effects of ryanodine have been confirmed using tetracaine which blocks ryanodine-sensitive Ca^{2+} release in the rabbit urethra [88, 90] and corporal tissue of the guinea pig penis [91]. In 17 ASMCs from six preparations of mouse renal pelvis bathed in 1 μM nifedipine and 100 μM Ni^{2+}, tetracaine (100 μM) reduces the amplitude and integral of their Ca^{2+} transients by only 22.2 ± 3.4% and 22.7 ± 3.3%, respectively, while their ½ width and frequency (0.2 ± 1.4 and 33.5 ± 32.8%, respectively) are not significantly altered (Fig. 3.6).

3.5.3 Interstitial Cells

A third pattern of action potential activity has been recorded in both the mouse and guinea pig renal pelvis. These action potentials display particularly long plateaus, occur at a frequency of 0.2–1 min^{-1}, are not associated with TSMC contraction [77] and have been demonstrated to arise

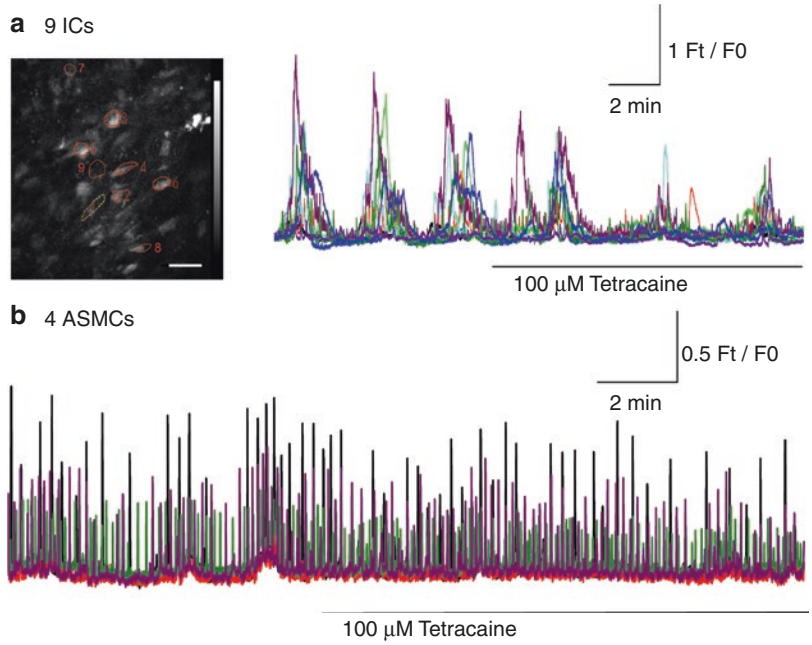

Fig. 3.6 IC Ca^{2+} transient activity and synchronicity (**a**) are more sensitive than ASMC Ca^{2+} transients (**b**) to tetracaine or ryanodine, blockers of CICR from internal stores. Ca^{2+} transient activity (F_t/F_0) in 9 ICs (**a** ROIs 1–9) and 4 ASMCs in a separate experiment (**b**) plotted against time (*t*), preparations bathed in 1 μM nifedipine: 100 μM Ni^{2+}-containing physiological salt solution. Scale bar in **a** left panel represents 50 μm

from irregular-shaped ICs [8, 24]. During intracellular microelectrode impalements, IC action potentials and STDs can be recorded concurrently with TSMC actions potentials. STDs and residual IC depolarizations ('slow waves') (Fig.3.3d) can also readily be recorded after blockade of TSMC discharge with nifedipine [77]. These observations confirm that the cells generating all three electrical events are electrically coupled in a syncytium and that the varying amplitude and time course of STDs and IC action potentials merely reflects the varying distance between the site of their generation in the syncytium and the recording electrode.

Upon blockade of TSMC Ca^{2+} signalling and contraction in the mouse renal pelvis, IC Ca^{2+} transients are mostly recorded in the bulb region and in regions more distal [77, 89]. Previously the use of fluo-4 reveals only a few (1–5) ICs displaying Ca^{2+} transients per field of view (×40–60 magnification) [77]. More recently, the use of Cal 520 with its grater fluorescence, penetration and loading reveals that each field of view contained many more ICs (Fig. 3.4) [3] (see Supplementary Video 3.2). Upon blockade of LDVCCs and TVDCCs with 1 μM nifedipine and 100 μM Ni^{2+}, IC Ca^{2+} transients separated by 20–200 μm fire asynchronously, but display synchronized bursting behaviour every 3–5 min (Figs. 3.5 and 3.6) [3]. The parameters of the time course of IC Ca^{2+} transients *between bursts* are best described by two Gaussian distributions, firing at frequencies of 1.1 and 3.5 min^{-1}, respectively (Fig. 3.5bi–biv), suggesting the presence of two populations of ICs [3]. However, the low frequencies of discharge of these two IC populations during our recording periods (typically 10–20 min) has not allowed any further discrimination based on their sensitivity to test agents.

3.6 Pacemaker Mechanisms in ASMCs and ICs

3.6.1 ASMCs

It seems likely that the initial trigger of the ASMC pacemaker signal involves the spontaneous release of a 'packet' of Ca^{2+} from internal stores that triggers the opening of a small number of Ca^{2+}-activated inward channels, resulting in a small 'unitary' STD and the influx of Ca^{2+}

through a nifedipine-insensitive Ca^{2+} pathway [78]. The 50% decrease in frequency but not blockade of ASMC Ca^{2+} transient firing when 100 μM Ni^{2+} is added to the mouse renal pelvis exposed to only nifedipine [3] suggests that Ca^{2+} entering through TVDCCs enhances a more global release of Ca^{2+} from sarcoplasmic/endoplasmic reticulum stores via Ca^{2+} release channels coupled to both IP_3 receptors and ryanodine receptors using Ca^{2+}-induced Ca^{2+} release (CICR) mechanisms [78, 92]. In the absence of LDVCC blockade, this entrainment would result in more frequent and larger ASMC Ca^{2+} transients and the summation of larger STDs into pacemaker potentials large enough to trigger the opening of TSMC LDVCCs, the firing of regenerative action potentials (Fig. 3.3bii) and the propagation of Ca^{2+} waves and contraction [77, 93].

3.6.2 ICs

Ca^{2+} transients in ICs in the same field of view are equally sensitive as ASMCs to the removal of Ca^{2+} from the bathing solution, blockade of SERCA with cyclopiazonic acid or the blockade of IP_3 receptor signalling with 2-APB [78]. However, in contrast to ASMC's partial sensitive sensitivity to ryanodine, IC Ca^{2+} transient discharge and their bursting behaviour are completely abolished by ryanodine [78] or profoundly reduced in tetracaine (Fig. 3.6a). This suggests that ICs differ fundamentally from ASMCs in their greater dependence on Ca^{2+} influx through TDVCCs and CICR from ryanodine-sensitive Ca^{2+} release channels.

This apparent greater dependence of IC Ca^{2+} signalling on CICR from ryanodine-sensitive stores and nifedipine-insensitive Ca^{2+} entry has been examined using various concentrations of the TVDCC blocker Ni^{2+}. Given the 70-fold difference in the IC_{50} of Ni^{2+} for $Ca_V3.2$ and $Ca_V3.1$ channels (5 and 350 μM, respectively) [85], the near complete blockade of TSMC Ca^{2+} waves and contraction in the presence of 10 μM Ni^{2+} plus nifedipine suggests the presence of active $Ca_V3.2$ channels in the TSMC layer. In addition, 100 μM Ni^{2+} would be expected to completely block $Ca_V3.2$ channels, but only partially block $Ca_V3.1$ channels. IC Ca^{2+} transients in the presence of 100 μM Ni^{2+} plus nifedipine are abolished upon the addition of the HCN channel blocker, ZD7288 [3]. Blockade of HCN channels may well lead to IC hyperpolarization to potentials negative of the opening threshold of any residual $Ca_V3.1$ channels and reduce Ca^{2+} entry. The co-location of immunoreactive product for HCN3 and $Ca_V3.1$ [39] in sub-urothelial ICs in the mouse proximal renal pelvis [3] suggests that voltage-dependent Ca^{2+} entry through $Ca_V3.1$ channels which triggers CICR from ryanodine-sensitive internal Ca^{2+} stores is essential for IC Ca^{2+} signalling [78], and that HCN3 channel-mediated depolarization contributes to the opening of these Ca^{2+} channels [93, 94]. However, single ICs of the mouse renal pelvis have not yet been demonstrated electrophysiologically to display either $Ca_V3.1$ or HCN currents [5], even though TVDCC currents have been recorded in prostatic and urethral myocytes [95] and HCN currents in cultured mouse dorsal root ganglia (RJ Lang unpublished data) under similar conditions.

3.7 IC Modulation of ASMCs

When bathed in 1 μM nifedipine and 100 μM Ni^{2+}, the most distinguishing property of the ICs was their ability to convert their asynchrony activity into synchronous bursts every 3–5 min (Fig. 3.5aii) [3]. This bursting behaviour occurs in cells that have no apparent close appositions, being often separated by 20–200 μm (Figs. 3.5ai and 3.6a). These bursts of IC Ca^{2+} transients also correlate in time with the accelerated activity and change in baseline of ASMCs within the same field of view (see Supplementary Video 3.2). This periodic acceleration of ASMC Ca^{2+} transient firing is blocked when IC Ca^{2+} transients are reduced by teracaine (Fig. 3.6b) or when gap junction cell-to-cell coupling is blocked by carbenoxolone [3]. However, the asynchronous firing of both cell types remains in carbenoxolone, albeit at a reduced level [3, 96]. Thus, it appears that ICs enhance the firing of neighbouring

ASMCs. A small increase in TSMC basal Ca^{2+} is also sometimes observed during these bursts of IC Ca^{2+} transients [3] which presumably also raises the excitability of the smooth muscle layer.

In the presence of both LVDCC and TVDCC blockers, the spread of excitation between ICs and their neighbours is likely to be intercellular and slowly voltage dependent, arising solely from the Ca^{2+}-activated membrane currents triggered by the spontaneous IC Ca^{2+} transients [5]. In the absence of LDVCC blockade, additional Ca^{2+} influx may well result in spontaneous IC Cl^--selective depolarizations that are more frequent and larger, which more effectively accelerate ASMC activity. They may even provide a constant influence on ASMC STD firing. As the number of ASMCs and ICs decrease and increase, respectively, with distance from the papilla pelvis border this IC influence may also increase with distance; even take over in the absence of a proximal pacemaker drive, i.e. act as 'latent pacemakers'.

3.8 Promoters of Pyeloureteric Peristalsis

3.8.1 Prostaglandins

It is well established that the intrinsic release of prostaglandins (PGs) is essential for maintaining spontaneous or evoked contractions in the upper urinary tract [24, 97]. The application of prostanoids has both positive and negative effects on upper urinary tract contractility. Applied $PGF_{2\alpha}$ tends to have an excitatory action on contractility in the upper urinary tract, PGE_1 tends to be inhibitory, while the effects of PGE_2 are more variable [24, 97]. In contrast, inhibition of PG synthesis with indomethacin decreases the spontaneous contractility in the renal pelvis and the spontaneous or evoked contractions in the ureter of various laboratory animals and human [24, 97], as well as reduces the release of cyclooxygenase products such as $PGF_{2\alpha}$, 6-keto $PGF_{1\alpha}$, PGI_2 and thromboxane $B_{2\alpha}$ [98, 99]. This blockade of contractility in the mouse and guinea pig renal pelvis does not arise from a blockade of conduction pathways as originally suggested by Thulelius et al. [28]. Blockers of cell-to cell coupling, 18β-glycyrrhetinic acid and carbenoxolone, rapidly prevent the propagation of action potentials, Ca^{2+} waves and contractions in the TSMC layer [3, 96]. In contrast, TSMC action potential discharge and contraction in the presence of indomethacin can readily be restored by nerve stimulation or the $PGF_{2\alpha}$ analogue, dinoprost [75].

The indomethacin-induced decrease in contractility in the renal pelvis arises from a decrease in the duration and frequency of the spontaneous action potentials due to an increase in the failures of underlying STDs to trigger an action potential [75]. In the mouse renal pelvis, the firing and synchronous bursting of IC Ca^{2+} transients are markedly reduced by indomethacin, which is associated with a 37–46% reduction in the amplitude and frequency of ASMC Ca^{2+} transients (Fig. 3.7b) [3] and a near complete blockade of their IC-evoked bursting behaviour (Fig. 3.7a). This reduction in ASMC Ca^{2+} transients presumably reduces the frequency and amplitude of the Ca^{2+}-activated membrane conductances underlying STD discharge and summation, essential for the triggering of TSMC action potential discharge. This reduction of IC Ca^{2+} transients, ASMC activity and pyeloureteric peristalsis upon cyclooxygenase inhibition suggests that their spontaneous activity is being fuelled by an autocrine/paracrine mechanism (Fig. 3.7c). It seems likely that locally released prostacyclins bind to G protein-coupled receptors on both ICs and ASMCs to contribute to the hydrolysis of phosphatidylinositol 4,5-bisphosphate (PIP_2) and IP_3 formation that drives their Ca^{2+} cycling [100].

A number of non-steroidal anti-inflammatory drugs (NSAIDs) which inhibit cyclooxygenase (COX)-arachidonic acid mediated production of eicosanoids also have various subunit-selective excitatory and inhibitory actions on $K_V7.x$ channels [101]. In the mouse renal pelvis, intense $K_V7.5$ immunoreactivity is present in BECs, while $Ano1^+$ ICs appear moderately $K_V7.5$ immuno-positive; both cells populations form close appositions with neighbouring TSMCs (Fig. 3.9). In single $K_V7.5^+$, $Ano1^+$ ICs from the

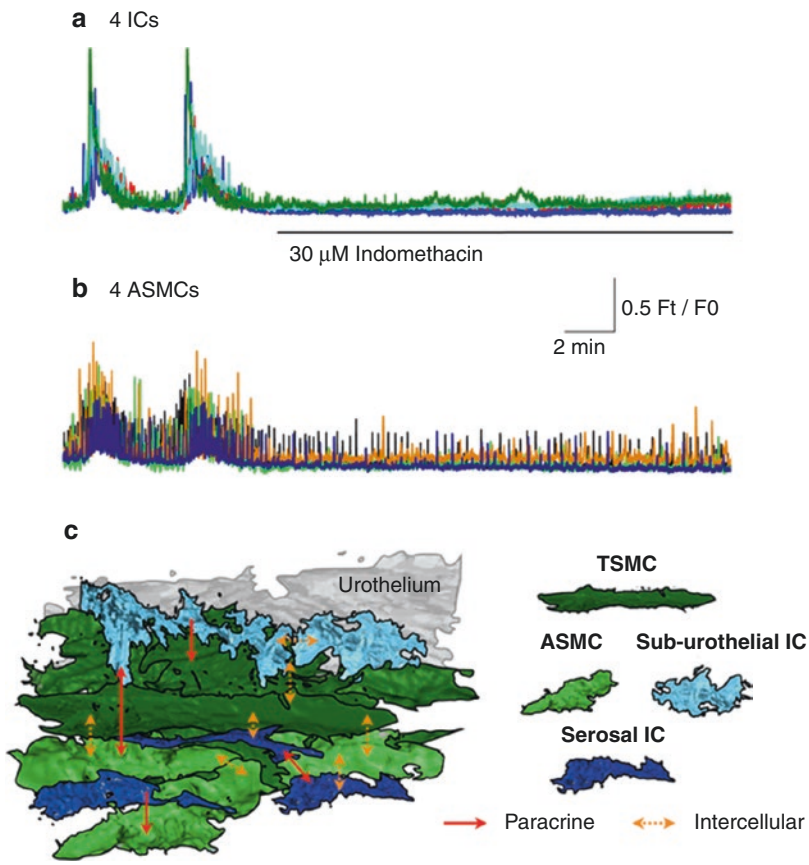

Fig. 3.7 Blockade of prostaglandin synthesis inhibits the firing and synchronous bursting of IC Ca^{2+} transients associated with a similar blockade of ASMC Ca^{2+} transient bursting, but only a 50% reduction in their amplitude and frequency. Ca^{2+} transient activity (F_t/F_0) in three 4 ICs (**a**) and 4 ASMCs (**b**) in the same field of view plotted against time (*t*). Preparation bathed in 1 μM nifedipine: 100 μM Ni^{2+}-containing physiological salt solution. (**c**) Schematic of paracrine (*red arrows*) and intercellular (*orange arrows*) pathways that ICs may modulate their own activity, ASMC pacemaking and TSMC contractility

mouse renal pelvis, the K_V7 channel modulator meclofenamic acid partially decreases an I_K that is abolished by the general K_V7 channel blocker, Xe991 [5]. K_V7 channel blockers Xe991 and linopirdine increase, while flupirtine a K_V7 channel activator decreases the frequency of TSMC contractions in the mouse renal pelvis. However, the excitatory effects of the linopirdine requires the previous blockade of intrinsic primary sensory nerves (PSNs) [2] as linopirdine also directly activates the capsaicin receptor TRPV1 [102]. The selective activation of $K_V7.2$ or $K_V7.4$ subunits with ML-213 (230–510 nM) also significantly decreases the amplitude and frequency of renal pelvis contractions in a manner reversed upon the addition of XE991 (M.J. Nguyen and R.J. Lang unpublished data). These preliminary pharmacological data suggest that native K_V7 ('m-current') channels in the renal pelvis are likely to be hetero-multimeric $K_V7.2$-5 channels constructs which have yet to be fully characterized or examined for their therapeutic potential.

3.8.2 Primary Sensory Nerves

The tonic release of neuropeptides from PSNs is essential for maintaining spontaneous activity in the renal pelvis [24, 97, 100]. Unmyelinated C-fibres and poorly myelinated Aδ-fibres [103] are distributed throughout the upper urinary tract of many mammals, innervating the adventitia, smooth muscle, epithelial layer and blood vessels [2, 104]. The relative proportion of immunoreactivity for tachykinins and calcitonin gene-related peptide (CGRP) neuropeptides are in equal quantities in nerve terminals of the guinea pig [105, 106] and human ureter [106, 107] but present in a ratio of 1:3, respectively, in rat ureter [105]. The rat renal pelvis also contains at least four distinct

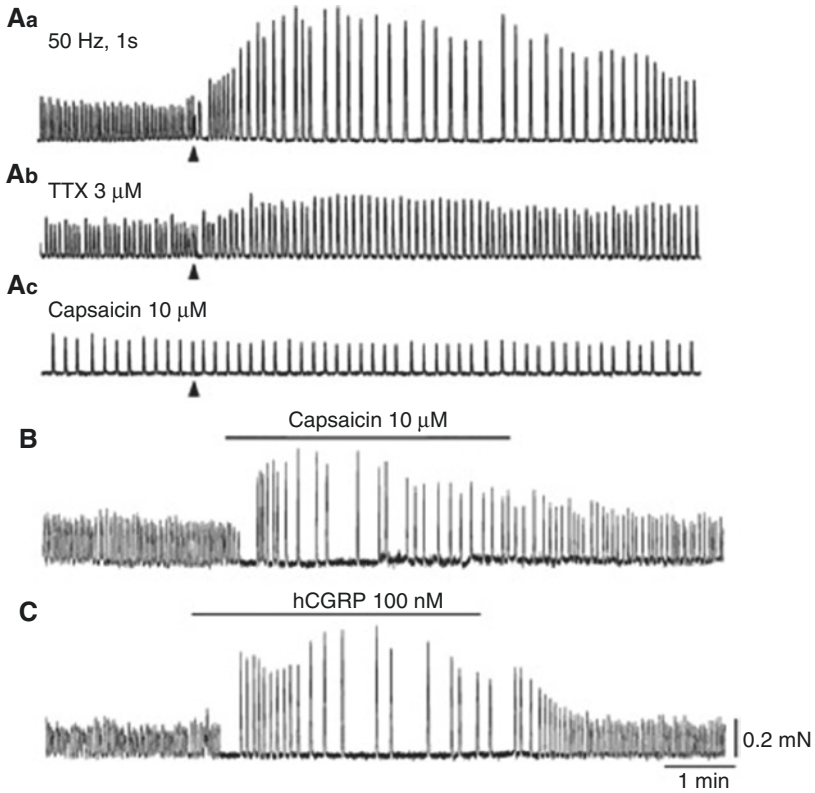

Fig. 3.8 Effects of primary sensory nerve (PSN) stimulation and bath-applied calcitonin gene-related peptide (CGRP) on spontaneous contractions of the mouse renal pelvis. Trains of PSN stimuli (50 Hz, 1 s; triangles) reduce the frequency but increase the amplitude of the spontaneous contractions (**Aa**). Tetrodotoxin (TTX 3 μM), reduces (**Ab**), while capsaicin (10 μM) completely blocks the effects of PSN stimulation (**Ac**). Capsaicin (10 μM) (**B**) and human CGRP (100 nM hCGRP) both have negative chronotropic and positive inotropic effects on the spontaneous contractions (**C**). Scale bars for **c** refer to all traces. Figure taken from Hashitani et al. [89]

populations of PSNs, based on their relative neuropeptide immunoreactivity [108].

Electrical stimulation of PSN terminals in the upper urinary tract [109] in vitro triggers action potentials which propagate into collateral branches, releasing neuropeptides in a manner relatively resistant to the sodium channel blocker tetrodotoxin (TTX) or the 'N-type' Ca^{2+} channel antagonist ω-conotoxin GVIA [110]. PSNs can also directly release and be depleted of their neuropeptides upon capsaicin binding to transient receptor potential vanilloid 1 (TRPV1) channels [89, 111] in a manner dependent on the age and species under investigation, and the method and number of administrations of capsaicin [22, 112–114].

Electrical or capsaicin stimulation of PSNs evokes a predominantly inhibitory effect on urinary tract motility in the rat [115] and guinea pig [116] ureter [110] and distal renal pelvis of the guinea pig [22]. In proximal renal pelvis of the guinea pig [22, 97] and mouse [89], PSN stimulation transiently increases and then inhibits contraction frequency, this prolonged negative chronotropic effects is associated with an increase in contraction amplitude and duration (Fig. 3.8Aa). In the guinea pig proximal renal pelvis, electrical field stimulation evokes a transient membrane depolarization in ASMCs [84] as well as a prolonged increase in the duration of TSMC action potentials in the distal renal pelvis [84] and ureter [72]. These positive ino-

tropic and chronotropic effects are reduced by the neurokinin A antagonist MEN 10376 suggesting they involve the release of excitatory neuropeptides, Neurokinin A and Substance P [22, 97, 117, 118].

Human CGRP (hCGRP) (Fig. 3.8C) and agents that increase internal cAMP levels [87, 89] mimic the PSN-mediated suppression of motility in the upper urinary tract (Fig. 3.8Aa) [89]. In the guinea pig ureter, the inhibitory effects of hCGRP are reduced in the presence of the blocker of ATP-dependent K^+ channels (K_{ATP}), glibenclamide, the cAMP antagonist, Rp-cAMPS or inhibitors of protein kinase A, H8 and H89 [119, 120]. In the mouse renal pelvis, glibenclamide also blocks the TSMC membrane hyperpolarization evoked by hCGRP or cAMP stimulators, but has little effect on their negative chronotropic and positive inotropic actions [87, 89]. Thus, the membrane potential-independent negative chronotropic effects of hCGRP arise mainly from the suppression of Ca^{2+} cycling in ASMCs via a cAMP-dependent second messenger system [89]. The positive inotropic effects of hCGRP may well be arising from the reduced TSMC action potential frequency which would promote Ca^{2+} store refilling, as well as TSMC hyperpolarization which would increase the availability and driving force of LDVCCs that contribute to the electrical discharge.

3.8.3 Autonomic Nerves

Extensive networks of parasympathetic, nitrergic [121] and sympathetic [122–124] nerves lie within the urothelial, submucosal, TSMC and serosal layers of the upper urinary tract. However, blockers of sympathetic, parasympathetic and nitrergic transmission or antagonists of α-adrenoceptors and muscarinic receptors have little effect on either renal pelvic autorhythmicity or the positive/negative inotropic and chronotropic effects evoked upon electrical or chemical stimulation of intrinsic nerves [15, 22, 86, 97, 117].

Activation of α-adrenoceptors with noradrenaline or adrenaline stimulates spontaneous contractions in the mouse [125], dog [126] and guinea pig [97] renal pelvis and in the pig ureter [36] associated with an increased Ca^{2+} influx during the prolongation of their action potential plateaus. In the guinea pig ureter, norepinephrine increases hydrolysis of PIP_2 and IP_3-dependent Ca^{2+} release from internal stores [127] which activates K^+ conductances that terminate the action potential plateau [97]. β-Adrenoceptor activation, membrane permeable cAMP analogues and inhibition of cAMP degradation [128] all reduce ureteric contractility [97] associated with a shortening of the action potential duration [129]. In the rabbit proximal renal pelvis, β-adrenoceptor activation has also been described to induce a positive inotropic effect [47, 97, 130, 131].

In comparison to other visceral smooth muscles, parasympathetic nerve stimulation or muscarinic receptor agonists have relatively little effect on pyeloureteric peristalsis. Exogenous application of acetylcholine increases contractility in the pig [132] and guinea pig [97] renal pelvis and the pig [133], human [134] and guinea pig [135] ureter, but has little effect on the porcine distal ureter [136]. Carbachol also decreases ureteric pressure and peristalsis in partially or completely obstructed ureters of anaesthetized dogs [137]. High concentrations of muscarinic receptor agonists have a robust negative chronotropic and positive inotropic effect on the spontaneous contractions in the mouse renal pelvis in a manner selectively prevented by either a nicotinic receptor antagonist or PSN depletion with capsaicin [125]. Glibenclamide also blocks this inhibition of pyeloureteric peristalsis, TSMC action potential firing and membrane hyperpolarization suggesting that carbachol activation of PSN nicotinic receptors leads to the release of CGRP that activates TSMC K_{ATP} channels [125].

The glibenclamide-independent inhibition of Ca^{2+} signalling in ASMCs upon PSN nicotinic receptor activation [125] may also arise from a reduction of the release of tachykinins essential

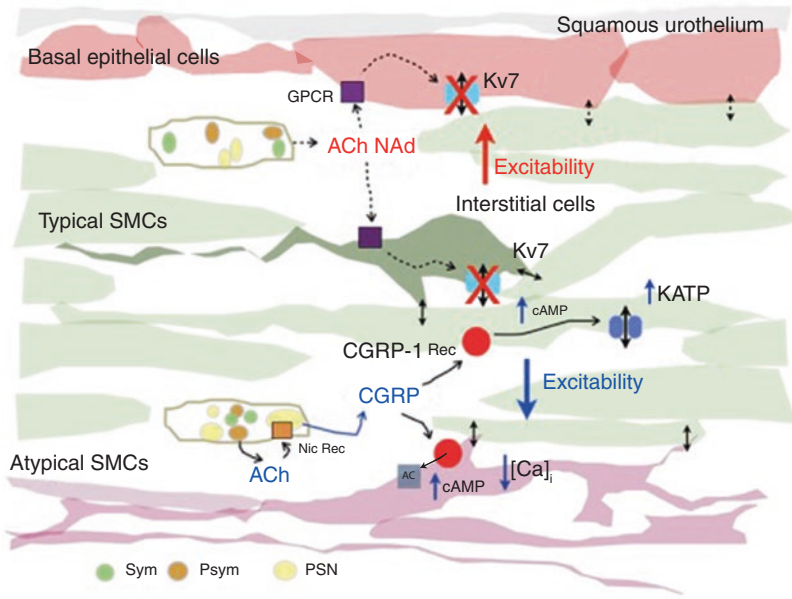

Fig. 3.9 Schematic of possible mechanisms of sympathetic (Sym), parasympathetic (Psym) and PSN modulation of pyeloureteric peristalsis. G protein-coupled receptor (GPCR) activation by acetylcholine (Ach), adrenaline (Ad) or tachykinins can lead to phospholipase C (PLC) metabolism and depletion of PIP2, KV7 channel closure (X) and membrane depolarization in BECs or ICs to increase the excitability of neighbouring electrically coupled ASMCs and TSMCs. Ach released from Psym nerves can also activate nicotinic receptors (Nic Rec) on neighbouring PSNs to release CGRP. This CGRP binds to its receptor (CGRP-1Rec) on both ASMCs and TSMCs to stimulate adenylyl cyclase (AC) and increase intracellular cAMP. In ASMCs, cAMP increases the Ca^{2+} buffering capacity of internal stores which reduces the intracellular cycling of Ca^{2+}, leading to an inhibition of ASMC Ca^{2+} transient discharge. This results in a decreased pacemaker drive and the observed decrease in frequency of contractions, action potentials and Ca^{2+} transients in TSMCs. The rise in cAMP in TSMCs leads to the opening of glibenclamide-sensitive K_{ATP} channels, resulting in membrane hyperpolarization that de-inactivates plasmalemmal Ca^{2+} channels. When a STD in a ASMC triggers an action potential in a neighbouring TSMC, the resulting Ca^{2+} transient and contraction may well be larger and longer than those observed in control

for sustaining pyeloureteric peristalsis. Alternatively, nicotinic receptor evoked release of CGRP may stimulate a cAMP-dependent increase in ASMC Ca^{2+} buffering that results in a reduction in the intracellular cycling of ASMC Ca^{2+} (Fig. 3.9) [100]. Thus, presynaptic PSN nicotinic receptors provide a means by which parasympathetic nerves can modulate the frequency and tone underlying pyeloureteric peristalsis. A combination of the inhibitory effects of PSN-released CGRP, a reduced release of tachykinins and TSMC muscarinic receptor evoked increases in the Ca^{2+} sensitivity of the contractile apparatus via a RhoA/Rho-associated kinase pathway [138] may well explain the often-contradictory effects of cholinergic agonists on the contractility of the upper urinary tract.

The autonomic and sensory innervation may also indirectly modulate the rate of conduction within and between ASMC and TSMC bundles by modulating the activity of neighbouring closely apposed $K_V7.5^+$ BECs or $K_V7.5^+$ ICs (Fig. 3.9) [2]. K_V7 channels require the presence of PIP_2 to remain open. Nerve-released tachykinins and autonomic neurotransmitters could well lead to a depletion of PIP_2 and K_V7 channel closure [139]. The by-products of PIP_2 metabolism, IP_3 and diacylglycerol (DAG) may also stimulate Ca^{2+} release and the activation of protein kinase C (PKC) which both lead to further inhibition of

K_V7.2-5 channels upon binding of Ca^{2+}-calmodulin and a protein kinase C (PKC)/A kinase anchoring protein (AKAP) complex [139]. Thus, closure of K_V7.5 channels in BECS and ICs may well remove a hyperpolarizing influence to increase the pacemaker drive in ASMCs as well as the ability of neighbouring TSMCs to initiate and conduct a wave of excitation (Fig. 3.9). It is interesting to speculate that $K_V7.5^+$ cells in the renal pelvis may control the frequency and size of the bolus at urine which enters the ureter from the renal pelvis in both uni-papilla and multi-papillae kidneys with changes in diuresis [40, 52], they may even control the establishment of the predominant minor calyx pacemaker in multi-papillae kidneys [32, 33, 36].

3.8.4 Renin-Angiotensin System

Angiotensin II acting exclusively on angiotensin receptor 1A (ATr1A) in mice evokes an increase in peristaltic contraction frequency that is associated with a rise in muscle wall tone and an increase in basal Ca^{2+} in both TSMCs and ASMCs [83]. ATr1A receptors are G protein-coupled receptors that leads to the production of G_{q11}-protein, activation of phospholipase C (PLC)–β and metabolism of PIP_2 to IP_3 and DAG [140]. ATr1 activation would therefore be expected to contribute to the intracellular IP_3 drive underlying cycling Ca^{2+} oscillators in both ICs and ASMCs.

3.9 Clinical Implications

Congenital hydronephrosis or ureteropelvic junction obstruction results in a compromised urine flow from the renal pelvis into the ureter that leads to pressure-induced dilatation of the renal collecting system and potential parenchyma injury which, if left untreated, results in renal disease and the development of salt-sensitive hypertension [141]. Renal pelvis dilatation is detected in 1 in 100 prenatal ultrasound screenings, with ureteropelvic junction obstruction being the most frequently diagnosed cause of antenatal hydronephrosis [142]. This hydronephrosis can be caused by a 'physical' stenosis, that usually requires *Anderson-Hynes* pyeloplasty, or by a 'functional' obstruction arising from a subtle developmental defect in the urothelium or muscle wall which usually disappears in 80% of infants within their 1st year [143, 144].

In children presenting with intrinsic ureteropelvic obstruction [62, 145], the site of dysfunction displays a decrease in the number of ASMCs and TSMCs, as well as a loss of their myofilaments and surface caveolae [146, 147]. Also evident is a marked collagen expression [145, 146, 148, 149], hyperplasia of the transitional epithelium [147, 150–152] and a decrease in the number of nerve terminals [145, 148, 149] and neuronal staining [64, 148, 149, 153, 154]. One electron microscopic examination of the structural integrity of ICs within hydronephrotic renal pelvises reports that their numbers are reduced and that their cytoplasm are enlarged with relatively few internal organelles [62]. A change of Kit staining, be it in nerve terminals or ICs, with ureteropelvic obstruction remains controversial; with reports that Kit immunoreactivity is only present in mast cells [155], that Kit staining increases [156], decreases [62, 64, 65] or little altered [157] with obstruction.

Little is known of the effects of hydronephrosis on the initiation or maintenance of pyeloureteric peristalsis. Mice lacking the Atr1A ($ATr1A^{-/-}$) present with a functional ureteropelvic obstruction associated with a hypoplastic papilla and renal cortex, a dilated calyx, proliferating and apoptotic tubulointerstitial cells, macrophage infiltration and fibrosis [158–160]. Mildly-to-moderately hydronephrotic kidneys in $ATr1A^{-/-}$ mice display spontaneous propagating contractions in their pelvic wall similar in frequency, but smaller in amplitude to their control ($ATr1A^{+/+}$, $ATr2^{+/+}$ and $ATr2^{-/-}$) mice [83]. However, the renal pelvis of severely hydronephrotic $ATr1A^{-/-}$ kidneys do not show any pyeloureteric contractile activity due to the complete destruction of the TSMC wall. Thus, the development of a functional obstruction in the

ureteropelvic junction of ATr1A$^{-/-}$ mice does not arise from a lack of development of the pyeloureteric pacemaker and contractile mechanisms [161]. It is more likely that the failure to transmit peristaltic contractions through the obstructed region of the proximal ureter in time leads to the development of back pressure-induced dilatation, apoptosis and fibrosis of the renal pelvis wall and kidney parenchyma [83].

Given the tendency of neonatal renal pelvis dilatation to resolve in the 1st few years after birth, it seems likely that in utero manipulation of the mechanisms that develop, drive or modulate pyeloureteric peristalsis has little therapeutic potential. Post birth, persistent dilatation of the renal pelvis arising from pyeloureteric stenosis can be closely monitored using ultrasound, magnetic resonance imaging or other voiding techniques to establish the necessity of further treatment or the timing of pyeloplasty surgery [162].

On the other hand, the control of pain, stone expulsion and prevention of kidney damage during renal colic already appears to involve many of the mechanism discussed herein. During renal colic, PSN mechanoceptors and chemoceptors in the renal pelvis and upper ureter transmit renal pain via C-fibres and Aδ-fibres to the dorsal horn of the spinal cord, then more centrally to supraspinal structures and the cerebral cortex. Convergence with other somatovisceral signals result in pain radiation to other visceral regions, as well as symptoms such as nausea, tachycardia and reduced gastrointestinal peristalsis [163]. Opiates provide rapid pain relief but also have excitatory contractile effects and appear to be no more effective than NSAIDs. The dependence of renal blood flow, glomerular filtration rate, pyeloureteric peristalsis etc., on prostaglandin, angiotensin and thromboxane A_2 [163] informs the use of NSAIDs for pain relief, but may have detrimental effects in patients with pre-existing renal disease. Interestingly, COX-2 inhibitors reduce ureteric peristalsis without gastric side effects. The short-term pain relief with nifedipine is associated with reduction of ureteric spasm without altering contraction frequency [163], consistent with the effects of LDVCC blockade described above [3]. While anticholinergic agents have proven not to be very useful, the muscle wall relaxation upon inhibition of α1D-adrenoceptors accelerates stone expulsion and reduces the use of analgesics [163]. Thus, there is potential to further refine the therapeutic selectivity of these drug groups upon a greater understanding of their actions in the upper urinary tract. Elucidation of the mechanisms by which ASMCs and ICs control contractility in the upper urinary tract under physiological and pathological conditions may also lead to the development of pharmacological interventions to improve outcomes in hydronephrotic infants and adults. However, future therapies to modulate pyeloureteric peristalsis will need to allow for any central, peripheral and systemic effects, as well as the degree and duration of pelviureteric blockade.

Acknowledgements The authors acknowledge the use of the imaging facilities within the Multi-modal Australian ScienceS Imaging and Visualization Environment (MASSIVE) at the Monash University node of the National Imaging Facility.

References

1. Walsberg GE. Small mammals in hot deserts: some generalizations revisited. Bioscience. 2000;50:109–20.
2. Nguyen MJ, Higashi R, Ohta K, Nakamura KI, Hashitani H, Lang RJ. Autonomic and sensory nerve modulation of peristalsis in the upper urinary tract. Auton Neurosci. 2016;200:1–10.
3. Hashitani H, Nguyen MJ, Noda H, Mitsui R, Higashi R, Ohta K, et al. Interstitial cell modulation of pyeloureteric peristalsis in the mouse renal pelvis examined using FIBSEM tomography and calcium indicators. Pflugers Arch. 2017;469:797–813.
4. Dixon JS, Gosling JA. Electron microscopic observations on the renal caliceal wall in the rat. Zeitschrift Fur Zellforschung Und Mikroskopische Anatomie. 1970;103:328–40.
5. Iqbal J, Tonta MA, Mitsui R, Li Q, Kett M, Li J, et al. Potassium and ANO1/TMEM16A chloride channel profiles distinguish atypical and typical smooth muscle cells from interstitial cells in the mouse renal pelvis. Br J Pharmacol. 2012;165:2389–408.
6. Gosling JA, Dixon JS. Species variation in the location of upper urinary tract pacemaker cells. Investig Urol. 1974;11:418–23.
7. Schmidt-Nielsen B. The renal pelvis. Kidney Int. 1987;31:621–8.

8. Klemm MF, Exintaris B, Lang RJ. Identification of the cells underlying pacemaker activity in the guinea-pig upper urinary tract. J Physiol. 1999;519:867–84.
9. Dixon JS, Gosling JA. The fine structure of pacemaker cells in the pig renal calices. Anat Rec. 1973;175:139–53.
10. Dixon JS, Gosling JA. The musculature of the human renal calices, pelvis and upper ureter. J Anat. 1982;135:129–37.
11. Gosling JA, Dixon JS. Morphologic evidence that the renal calyx and pelvis control ureteric activity in the rabbit. Am J Anat. 1971;130:393–408.
12. Dixon JS, Gosling JA. Fine structural observations on the attachment of the calix to the renal parenchyma in the rat. J Anat. 1970;106:181–2.
13. Lang RJ, Klemm MF. Interstitial cell of Cajal-like cells in the upper urinary tract. J Cell Mol Med. 2005;9:543–56.
14. Englemann TW. Zur Physiologie des Ureter. Pflugers Arch Ges Physiol. 1869;2:243–93.
15. Golenhofen K, Hannappel J. Normal spontaneous activity of the pyeloureteral system in the guinea-pig. Pflugers Arch. 1973;341:257–70.
16. Morita T. The in vitro study of the pacemaker activity of the canine renal pelvis throughout simultaneous recordings of pelvic pressure changes and electromyogram on various regions of the renal pelvis. Nihon Hinyokika Gakkai Zasshi. 1978;69:304–14.
17. Tsuchida S, Morita T, Yamaguchi O. The simultaneous recording of the rhythmic contraction and electrical activity of the renal previs—a new in vitro method. Tohoku J Exp Med. 1978;124:93–4.
18. Longrigg N. Minor calyces as primary pacemaker sites for ureteral activity in man. Lancet. 1975;1:253–4.
19. Weiss R, Wagner ML, Hoffman BF. Localization of the pacemaker for peristalsis in the intact canine ureter. Investig Urol. 1967;5:42–8.
20. Weiss RM, Tamarkin FJ, Wheeler MA. Pacemaker activity in the upper urinary tract. J Smooth Muscle Res. 2006;42:103–15.
21. Dwyer TM, Schmidt-Nielsen B. The renal pelvis: machinery that concentrates urine in the papilla. News Physiol Sci. 2003;18:1–6.
22. Teele ME, Lang RJ. Stretch-evoked inhibition of spontaneous migrating contractions in a whole mount preparation of the Guinea-pig upper urinary tract. Brit J Pharmacol. 1998;123:1143–53.
23. Lang RJ, Takano H, Davidson ME, Suzuki H, Klemm MF. Characterization of the spontaneous electrical and contractile activity of smooth muscle cells in the rat upper urinary tract. J Urol. 2001;166:329–34.
24. Lang RJ, Davidson ME, Exintaris B. Pyeloureteral motility and ureteral peristalsis: essential role of sensory nerves and endogenous prostaglandins. Exp Physiol. 2002;87:129–46.
25. Bozler E. The activity of the pacemaker previous to the discharge of a muscular impulse. Am J Phys. 1942;136:543–52.
26. Hannappel H, Golenhofen K. Comparative studies on normal ureteral peristalsis in dogs, guinea-pigs and rats. Pflugers Arch. 1974;348:65.
27. Djurhuus JC. Dynamics of upper urinary tract. III. The activity of renal pelvis during pressure variations. Investig Urol. 1977;14:475–7.
28. Thulesius O, Ugaily-Thulesius L, Angelo-Khattar M. Generation and transmission of ovine ureteral contractions, with special reference to prostaglandins. Acta Physiol Scand. 1986;127:485–90.
29. Gosling JA, Constantinou CE. The origin and propagation of upper urinary tract contraction waves. A new in vitro methodology. Experientia. 1976;32:266–7.
30. Yamaguchi O, Constantinou CE. Renal calyceal and pelvic contraction rhythms. Am J Phys. 1989;257:R788–95.
31. Constantinou CE. Renal pelvic pacemaker control of ureteral peristaltic rate. Am J Phys. 1974;226:1413–9.
32. Constantinou CE, Silvert MA, Gosling J. Pacemaker system in the control of ureteral peristaltic rate in the multicalyceal kidney of the pig. Investig Urol. 1977;14:440–1.
33. Morita T, Ishizuka G, Tsuchida S. Initiation and propagation of stimulus from the renal pelvic pacemaker in pig kidney. Investig Urol. 1981;19:157–60.
34. Tsuchida S, Morita T, Harada T, Kimura Y. Initiation and propagation of canine renal pelvic peristalsis. Urol Int. 1981;36:307–14.
35. Constantinou CE, Yamaguchi O. Multiple-coupled pacemaker system in renal pelvis of the unicalyceal kidney. Am J Phys. 1981;241:412–8.
36. Hannappel H, Golenhofen K, Hohnsbein J, Lutzeyer W. Pacemaker process of ureteral peristalsis in multicalyceal kidneys. Urol Int. 1982;37:240–6.
37. Lammers WJ, Ahmad HR, Arafat K. Spatial and temporal variations in pacemaking and conduction in the isolated renal pelvis. Am J Phys. 1996;270:F567–74.
38. Hurtado R, Bub G, Herzlinger D. The pelvis-kidney junction contains HCN3, a hyperpolarization-activated cation channel that triggers ureter peristalsis. Kidney Int. 2010;77:500–8.
39. Hurtado R, Bub G, Herzlinger D. A molecular signature of tissues with pacemaker activity in the heart and upper urinary tract involves coexpressed hyperpolarization-activated cation and T-type Ca^{2+} channels. FASEB J. 2014;28:730–9.
40. Constantinou CE, Hrynczuk JR. The incidence of ecotpic peristaltic contractions. Urol Int. 1976;31:476–88.
41. Davidson ME, Lang RJ. Effects of selective inhibitors of cyclo-oxygenase-1 (COX-1) and cyclo- oxygenase-2 (COX-2) on the spontaneous myogenic contractions in the upper urinary tract of the guinea-pig and rat. Br J Pharmacol. 2000;129:661–70.
42. Shiratori T, Kinoshita H. Electromyographic studies on urinary tract. II. Electromyographic study on the genesis of peristaltic movement of the dog's ureter. Tohoku J Exp Med. 1961;73:103–17.

43. Morita T, Kondo S, Suzuki T, Ichikawa S, Tsuchida S. Effect of calyceal resection on pelviureteral peristalsis in isolated pig kidney. J Urol. 1986;135:151–4.
44. Hannappel J, Lutzeyer W. Pacemaker localization in the renal pelvis of the unicalyceal kidney. In vitro study in the rabbit. Eur Urol. 1978;4:192–4.
45. Constantinou CE. Contractility of the pyeloureteral pacemaker system. Urol Int. 1978;33:399–416.
46. Constantinou CE, Neubarth JL, Mensah-Dwumah M. Frequency gradient in the autorhythmicity of the pyeloureteral pacemaker system. Experientia. 1978;34:614–5.
47. Morita T. Characteristics of spontaneous contraction and effects of isoproterenol on contractility in isolated rabbit renal pelvic smooth muscle strips. J Urol. 1986;135:604–7.
48. Longrigg N. In vitro studies on smooth muscle of the human renal pelvis. Eur J Pharmacol. 1975;34:293–8.
49. Weiss RM, Bassett AL, Hoffman BF. Dynamic length-tension curves of cat ureter. Am J Phys. 1972;222:388–93.
50. Thulesius O, Angelo-Khattar M, Sabha M. The effect of ureteral distension on peristalsis. Studies on human and sheep ureters. Urol Res. 1989;17:385–8.
51. Potjer RM, Kimoto Y, Constantinou CE. Topological localization of the frequency and amplitude characteristics of the whole and segmented renal pelvis. Urol Int. 1992;48:278–83.
52. Constantinou CE, Hrynczuk JR. Urodynamics of the upper urinary tract. Investig Urol. 1976;14:233–40.
53. Lang RJ, Zhang Y. The effects of K^+ channel blockers on the spontaneous electrical and contractile activity in the proximal renal pelvis of the guinea pig. J Urol. 1996;155:332–6.
54. Hurtado R, Smith CS. Hyperpolarization-activated cation and T-type calcium ion channel expression in porcine and human renal pacemaker tissues. J Anat. 2016;228:812–25.
55. Metzger R, Schuster T, Till H, Franke FE, Dietz HG. Cajal-like cells in the upper urinary tract: comparative study in various species. Pediatr Surg Int. 2005;21:169–74.
56. Metzger R, Neugebauer A, Rolle U, Bohlig L, Till H. C-Kit receptor (CD117) in the porcine urinary tract. Pediatr Surg Int. 2008;24(1):67–76.
57. Metzger R, Schuster T, Till H, Stehr M, Franke FE, Dietz HG. Cajal-like cells in the human upper urinary tract. J Urol. 2004;172:769–72.
58. van der Aa F, Roskams T, Blyweert W, Ost D, Bogaert G, De Ridder D. Identification of kit positive cells in the human urinary tract. J Urol. 2004;171:2492–6.
59. Pezzone MA, Watkins SC, Alber SM, King WE, de Groat WC, Chancellor MB, et al. Identification of c-kit-positive cells in the mouse ureter: the interstitial cells of Cajal of the urinary tract. Am J Physiol Ren Physiol. 2003;284:F925–9.
60. David SG, Cebrian C, Vaughan ED, Herzlinger D. C-kit and ureteral peristalsis. J Urol. 2005;173:292–5.
61. Arena S, Fazzari C, Arena F, Scuderi MG, Romeo C, Nicotina PA, et al. Altered 'active' antireflux mechanism in primary vesico-ureteric reflux: a morphological and manometric study. BJU Int. 2007;100:407–12.
62. Eken A, Erdogan S, Kuyucu Y, Seydaoglu G, Polat S, Satar N. Immunohistochemical and electron microscopic examination of Cajal cells in ureteropelvic junction obstruction. Can Urol Assoc J. 2013;7:E311–6.
63. Cain JE, Islam E, Haxho F, Blake J, Rosenblum ND. GLI3 repressor controls functional development of the mouse ureter. J Clin Invest. 2011;121:1199–206.
64. Solari V, Piotrowska AP, Puri P. Altered expression of interstitial cells of Cajal in congenital ureteropelvic junction obstruction. J Urol. 2003;170:2420–2.
65. Yang X, Zhang Y, Hu J. The expression of Cajal cells at the obstruction site of congenital pelviureteric junction obstruction and quantitative image analysis. J Pediatr Surg. 2009;44:2339–42.
66. Zhu MH, Kim TW, Ro S, Yan W, Ward SM, Koh SD, et al. A Ca^{2+}-activated Cl^- conductance in interstitial cells of Cajal linked to slow wave currents and pacemaker activity. J Physiol. 2009;587:4905–18.
67. Kobayashi M. Relationship between membrane potential and spike configuration recorded by sucrose gap method in the ureter smooth muscle. Comp Biochem Physiol. 1971;38A:301–8.
68. Zawalinski VC, Constantinou CE, Burnstock G. Ureteral pacemaker potentials recorded with the sucrose gap technique. Experientia. 1975;31:931–3.
69. Santicioli P, Maggi CA. Pharmacological modulation of electromechanical coupling in the proximal and distal regions of the guinea-pig renal pelvis. J Auton Pharmacol. 1997;17:43–52.
70. Irisawa H, Kobayashi M. Effects of repetitive stimuli and temperature on ureter action potentials. Jpn J Physiol. 1963;13:421–30.
71. Kuriyama H, Osa T, Toida N. Membrane properties of the smooth muscle of guinea-pig ureter. J Physiol. 1967;191:225–38.
72. Exintaris B, Lang RJ. Effects of nerve stimulation on spontaneously active preparations of the guinea pig ureter. Urol Res. 1999;27:328–35.
73. Exintaris B, Lang RJ. K(+) channel blocker modulation of the refractory period in spontaneously active guinea-pig ureters. Urol Res. 1999;27:319–27.
74. Tsuchida S, Suzuki T. Pacemaker activity of the pelvicalyceal border recorded by an intracellular glass microelectrode. Urol Int. 1992;48:121–4.
75. Zhang Y, Lang RJ. Effects of intrinsic prostaglandins on the spontaneous contractile and electrical activity of the proximal renal pelvis of the guinea-pig. Br J Pharmacol. 1994;113:431–8.
76. Kobayashi M. Effect of calcium on electrical activity in smooth muscle cells of cat ureter. Am J Phys. 1969;216:1279–85.
77. Lang RJ, Hashitani H, Tonta MA, Parkington HC, Suzuki H. Spontaneous electrical and Ca^{2+} signals in

typical and atypical smooth muscle cells and interstitial cell of Cajal-like cells of mouse renal pelvis. J Physiol. 2007;583:1049–68.
78. Lang RJ, Hashitani H, Tonta MA, Suzuki H, Parkington HC. Role of Ca^{2+} entry and Ca^{2+} stores in atypical smooth muscle cell autorhythmicity in the mouse renal pelvis. Br J Pharmacol. 2007;152:1248–59.
79. Takano H, Nakahira Y, Suzuki H. Properties of spontaneous electrical activity in smooth muscle of the guinea-pig renal pelvis. Jpn J Physiol. 2000;50:597–603.
80. Burdyga T, Wray S. Action potential refractory period in ureter smooth muscle is set by Ca sparks and BK channels. Nature. 2005;436:559–62.
81. Burdyga TV, Wray S. The relationship between the action potential, intracellular calcium and force in intact phasic, guinea-pig uretic smooth muscle. J Physiol. 1999;520:867.
82. Lang RJ, Hashitani H, Keller S, Takano H, Mulholland EL, Fukuta H, et al. Modulators of internal Ca^{2+} stores and the spontaneous electrical and contractile activity of the guinea-pig renal pelvis. Br J Pharmacol. 2002;135:1363–74.
83. Nguyen MJ, Hashitani H, Lang RJ. Angiotensin receptor-1A knockout leads to hydronephrosis not associated with a loss of pyeloureteric peristalsis in the mouse renal pelvis. Clin Exp Pharmacol Physiol. 2016;43:535–42.
84. Lang RJ, Zhang Y, Exintaris B, Vogalis F. Effects of nerve stimulation on the spontaneous action potentials recorded in the proximal renal pelvis of the guinea-pig. Urol Res. 1995;23:343–50.
85. Kang HW, Park JY, Jeong SW, Kim JA, Moon HJ, Perez-Reyes E, et al. A molecular determinant of nickel inhibition in Cav3.2 T-type calcium channels. J Biol Chem. 2006;281:4823–30.
86. Lang RJ, Exintaris B, Teele ME, Harvey J, Klemm MF. Electrical basis of peristalsis in the mammalian upper urinary tract. Clin Exp Pharmacol Physiol. 1998;25:310–21.
87. Lang RJ, Tonta MA, Zoltkowski BZ, Meeker WE, Wendt I, Parkington HC. Pyeloureteric peristalsis: role of atypical smooth muscle cells and interstitial cells of Cajal-like cells as pacemakers. J Physiol. 2006;576:695–705.
88. Johnston L, Sergeant GP, Hollywood MA, Thornbury KD, McHale NG. Calcium oscillations in interstitial cells of the rabbit urethra. J Physiol. 2005;565:449–61.
89. Hashitani H, Lang RJ, Mitsui R, Mabuchi Y, Suzuki H. Distinct effects of CGRP on typical and atypical smooth muscle cells involved in generating spontaneous contractions in the mouse renal pelvis. Br J Pharmacol. 2009;158:2030–45.
90. Hashitani H, Suzuki H. Properties of spontaneous Ca2+ transients recorded from interstitial cells of Cajal-like cells of the rabbit urethra in situ. J Physiol. 2007;583:505–19.
91. Hashitani H, Suzuki H. Identification of interstitial cells of Cajal in corporal tissues of the guinea-pig penis. Br J Pharmacol. 2004;14:199–204.
92. Miyakawa T, Mizushima A, Hirose K, Yamazawa T, Bezprozvanny I, Kurosaki T, et al. Ca^{2+}-sensor region of IP_3 receptor controls intracellular Ca^{2+} signaling. EMBO J. 2001;20:1674–80.
93. Lang RJ, Hashitani H, Tonta MA, Bourke JL, Parkington HC, Suzuki H. Spontaneous electrical and Ca^{2+} signals in the mouse renal pelvis that drive pyeloureteric peristalsis. Clin Exp Pharmacol Physiol. 2010;37:509–15.
94. Biel M, Wahl-Schott C, Michalakis S, Zong X. Hyperpolarization-activated cation channels: from genes to function. Physiol Rev. 2009;89:847–85.
95. Lang RJ, Tonta MA, Takano H, Hashitani H. Voltage-operated Ca^{2+} currents and Ca^{2+}-activated Cl^- currents in single interstitial cells of the guinea pig prostate. BJU Int. 2014;114:436–46.
96. Lang RJ, Zoltkowski BZ, Hammer JM, Meeker WF, Wendt I. Electrical characterization of interstitial cells of Cajal-like cells and smooth muscle cells isolated from the mouse ureteropelvic junction. J Urol. 2007;177:1573–80.
97. Santicioli P, Maggi CA. Myogenic and neurogenic factors in the control of pyeloureteral motility and ureteral peristalsis. Pharmacol Rev. 1998;50:683–722.
98. Thulesius O, Angelo-Khattar M, Ali M. The effect of prostaglandin synthesis inhibition on motility of the sheep ureter. Acta Physiol Scand. 1987;131:51–4.
99. Ali M, Angelo-Khattar M, Thulesius L, Fareed A, Thulesius O. Urothelial synthesis of prostanoids in the ovine ureter. Urol Res. 1998;26:171–4.
100. Lang RJ. Role of hyperpolarization-activated cation channels in pyeloureteric peristalsis. Kidney Int. 2010;77:483–5.
101. Peretz A, Degani-Katzav N, Talmon M, Danieli E, Gopin A, Malka E, et al. A tale of switched functions: from cyclooxygenase inhibition to M-channel modulation in new diphenylamine derivatives. PLoS One. 2007;2:e1332.
102. Neacsu C, Babes A. The M-channel blocker linopirdine is an agonist of the capsaicin receptor TRPV1. J Pharmacol Sci. 2010;114(3):332–40.
103. Ammons WS. Bowditch Lecture. Renal afferent inputs to ascending spinal pathways. Am J Phys. 1992;262:R165–76.
104. Amann R, Skofitsch G, Lembeck F. Species-related differences in the capsaicin-sensitive innervation of the rat and guinea-pig ureter. Naunyn Schmiedeberg's Arch Pharmacol. 1988;338:407–10.
105. Su HC, Wharton J, Polak JM, Mulderry PK, Ghatei MA, Gibson SJ, et al. Calcitonin gene-related peptide immunoreactivity in afferent neurons supplying the urinary tract: combined retrograde tracing and immunohistochemistry. Neuroscience. 1986;18:727–47.

106. Hua XY, Theodorsson-Norheim E, Lundberg JM, Kinn AC, Hokfelt T, Cuello AC. Co-localization of tachykinins and calcitonin gene-related peptide in capsaicin-sensitive afferents in relation to motility effects on the human ureter in vitro. Neuroscience. 1987;23:693–703.
107. Edyvane KA, Smet PJ, Trussell DC, Jonavicius J, Marshall VR. Patterns of neuronal colocalisation of tyrosine hydroxylase, neuropeptide Y, vasoactive intestinal polypeptide, calcitonin gene-related peptide and substance P in human ureter. J Auton Nerv Syst. 1994;48:241–55.
108. Ferguson M, Bell C. Ultrastructural localization and characterization of sensory nerves in the rat kidney. J Comp Neurol. 1988;274:9–16.
109. Maggi CA, Meli A. The sensory-efferent function of capsaicin-sensitive sensory neurons. Gen Pharmacol. 1988;19:1–43.
110. Maggi CA, Giuliani S. The neurotransmitter role of calcitonin gene-related peptide in the rat and guinea-pig ureter: effect of a calcitonin gene- related peptide antagonist and species-related differences in the action of omega conotoxin on calcitonin gene-related peptide release from primary afferents. Neuroscience. 1991;43:261–8.
111. Chung MK, Guler AD, Caterina MJ. TRPV1 shows dynamic ionic selectivity during agonist stimulation. Nat Neurosci. 2008;11:555–64.
112. Hua XY, Lundberg JM. Dual capsaicin effects on ureteric motility: low dose inhibition mediated by calcitonin gene-related peptide and high dose stimulation by tachykinins? Acta Physiol Scand. 1986;128:453–65.
113. Holzer P. Local effector functions of capsaicin-sensitive sensory nerve endings: involvement of tachykinins, calcitonin gene-related peptide and other neuropeptides. Neuroscience. 1988;24:739–68.
114. Maggi CA, Patacchini R, Santicioli P, Giuliani S, Del Bianco E, Geppetti P, et al. The ‘efferent’ function of capsaicin-sensitive nerves: ruthenium red discriminates between different mechanisms of activation. Eur J Pharmacol. 1989;170:167–77.
115. Maggi CA, Santicioli P, Giuliani S, Abelli L, Meli A. The motor effect of the capsaicin-sensitive inhibitory innervation of the rat ureter. Eur J Pharmacol. 1986;126:333–6.
116. Maggi CA, Giuliani S, Santicioli P. Multiple mechanisms in the smooth muscle relxant action of calcitonin gene-related peptide (CGRP) in the guinea-pig ureter. Naunyn Schmiedeberg's Arch Pharmacol. 1994;350:537–47.
117. Maggi CA, Theodorsson E, Santicioli P, Giuliani S. Tachykinins and calcitonin gene-related peptide as co- transmitters in local motor responses produced by sensory nerve activation in the guinea-pig isolated renal pelvis. Neuroscience. 1992;46:549–59.
118. Maggi CA, Astolfi M, Giuliani S, Goso C, Manzini S, Meini S, et al. MEN 10,627, a novel polycyclic peptide antagonist of tachykinin NK2 receptors. J Pharmacol Exp Ther. 1994;271:1489–500.
119. Maggi CA, Giuliani S, Meini S, Santicioli P. Calcitonin gene related peptide as inhibitory neurotransmitter in the ureter. Can J Physiol Pharmacol. 1995;73:986–90.
120. Maggi CA, Giuliani S, Santicioli P. CGRP inhibition of electromechanical coupling in the Guinea-pig isolated renal pelvis. Naunyn Schmiedeberg's Arch Pharmacol. 1995;352:529–39.
121. Rolle U, Chertin B, Nemeth L, Puri P. Demonstration of nitrergic and cholinergic innervation in whole-mount preparations of rabbit, pig, and human upper urinary tract. Pediatr Surg Int. 2002;18:315–8.
122. Gosling JA, Dixon JS. Catecholamine-containing nerves in the submucosa of the ureter. Experientia. 1971;27:1065–6.
123. Gosling JA, Dixon JS. The effect of 6-hydroxydopamine on nerves in the rat upper urinary tract. J Cell Sci. 1972;10(1):197–209.
124. Warburton AL, Santer RM. Sympathetic and sensory innervation of the urinary tract in young adult and aged rats: a semi-quantitative histochemical and immunohistochemical study. Histochem J. 1994;26:127–33.
125. Nguyen MJ, Angkawaijawa S, Hashitani H, Lang RJ. Nicotinic receptor activation on primary sensory afferents modulates autorhythmicity in the mouse renal pelvis. Br J Pharmacol. 2013;170:1221–32.
126. Morita T, Wada I, Suzuki T, Tsuchida S. Characterization of alpha-adrenoceptor subtypes involved in regulation of ureteral fluid transport. Tohoku Exp Med. 1987;152:111–8.
127. Wheeler MA, Martin TV, Weiss RM. Effect of carbachol and norepinephrine on phosphatidyl-inositol hydrolysis and cyclic-amp levels in guinea-pig urinary-tract. J Urol. 1995;153:2044–9.
128. Weiss RM, Vulliemoz Y, Verosky M, Rosen MR, Triner L. Adenylate cyclase and phosphodiesterase activity in rabbit ureter. Investig Urol. 1977;15:15–8.
129. Kovalev IV, Popov AG, Baskakov MB, Minochenko IL, Kilin AA, Borodin YL, et al. Effect of inhibitors of cyclic nucleotide phosphodiesterases on electrical and contractile activity of smooth muscle cells. Bull Exp Biol Med. 2002;133:38–40.
130. Morita T, Miyagawa I, Wheeler M, Weiss RM. Effect of isoproterenol on contractile force of isolated rabbit renal pelvic smooth muscle. Tohoku J Exp Med. 1985;147:153–5.
131. Kondo S, Morita T, Tsuchida S, Terui M, Tashima Y. Effect of dobutamine on adenylate cyclase activity in rabbit renal pelvis and ureter. Tohoku J Exp Med. 1986;148:113–4.
132. Sorensen SS, Husted SE, Nissen T, Djurhuus JC. Topographic variations in alpha-adrenergic and cholinergic response in the pig renal pelvis. Urol Int. 1983;38:271–4.
133. Hernandez M, Simonsen U, Prieto D, Rivera L, Garcia P, Ordaz E, et al. Different muscarinic

receptor subtypes mediating the phasic activity and basal tone of pig isolated intravesical ureter. Br J Pharmacol. 1993;110:1413–20.
134. Long S, Nergardh A. Autonomic receptor functions of the human ureter: an in vitro study. Scand J Urol Nephrol. 1978;12:23–6.
135. Yoshida S, Kuga T. Effects of field stimulation on cholinergic fibers of the pelvic region in the isolated guinea pig ureter. Jpn J Physiol. 1980;30:415–26.
136. Roshani H, Dabhoiwala NF, Dijkhuis T, Pfaffendorf M, Boon TA, Lamers WH. Pharmacological modulation of ureteral peristalsis in a chronically instrumented conscious pig model. I: effect of cholinergic stimulation and inhibition. J Urol. 2003;170:264–7.
137. Tomiyama Y, Wanajo I, Yamazaki Y, Kojima M, Shibata N. Effects of cholinergic drugs on ureteral function in anesthetized dogs. J Urol. 2004;172:1520–3.
138. Borysova L, Shabir S, Walsh MP, Burdyga T. The importance of Rho-associated kinase-induced Ca^{2+} sensitization as a component of electromechanical and pharmacomechanical coupling in rat ureteric smooth muscle. Cell Calcium. 2011;50:393–405.
139. Delmas P, Brown DA. Pathways modulating neural KCNQ/M (Kv7) potassium channels. Nat Rev Neurosci. 2005;6:850–62.
140. Higuchi S, Ohtsu H, Suzuki H, Shirai H, Frank GD, Eguchi S. Angiotensin II signal transduction through the AT1 receptor: novel insights into mechanisms and pathophysiology. Clin Sci. 2007;112:417–28.
141. Carlstrom M, Brown RD, Edlund J, Sallstrom J, Larsson E, Teerlink T, et al. Role of nitric oxide deficiency in the development of hypertension in hydronephrotic animals. Am J Physiol Ren Physiol. 2008;294:F362–70.
142. Chertin B, Pollack A, Koulikov D, Rabinowitz R, Shen O, Hain D, et al. Does renal function remain stable after puberty in children with prenatal hydronephrosis and improved renal function after pyeloplasty? J Urol. 2009;182:1845–8.
143. Schedl A. Renal abnormalities and their developmental origin. Nat Rev Genet. 2007;8:791–802.
144. Song R, Yosypiv IV. Genetics of congenital anomalies of the kidney and urinary tract. Pediatr Nephrol. 2011;26:353–64.
145. Kaya C, Bogaert G, de Ridder D, Schwentner C, Fritsch H, Oswald J, et al. Extracellular matrix degradation and reduced neural density in children with intrinsic ureteropelvic junction obstruction. Urology. 2010;76:185–9.
146. Gosling JA, Dixon JS. Functional obstruction of the ureter and renal pelvis. A histological and electron microscopic study. Br J Urol. 1978;50:145–52.
147. Faussone-Pellegrini MS, Rizzo M, Grechi G. Ultrastructural modifications of the tunica muscularis in congenital obstruction of the upper urinary tract. Physiopathological interpretations and anatomo-clinical correlations. J Urol (Paris). 1984;90:217–26.
148. Murakumo M, Nonomura K, Yamashita T, Ushiki T, Abe K, Koyanagi T. Structural changes of collagen components and diminution of nerves in congenital ureteropelvic junction obstruction. J Urol. 1997;157:1963–8.
149. Kajbafzadeh AM, Payabvash S, Salmasi AH, Monajemzadeh M, Tavangar SM. Smooth muscle cell apoptosis and defective neural development in congenital ureteropelvic junction obstruction. J Urol. 2006;176:718–23.
150. Baumgart P, Muller KM, Lison AE. Epithelial abnormalities in the renal pelvis in experimental hydronephrosis and pyelonephritis. Pathol Res Pract. 1983;176:185–95.
151. Chiou YY, Shieh CC, Cheng HL, Tang MJ. Intrinsic expression of Th2 cytokines in urothelium of congenital ureteropelvic junction obstruction. Kidney Int. 2005;67:638–46.
152. Stravodimos KG, Koritsiadis G, Lazaris AC, Agrogiannis G, Koutalellis G, Constantinides C, et al. Hydronephrosis promotes expression of hypoxia-inducible factor 1 alpha. Urol Int. 2009;82:38–42.
153. Wang Y, Puri P, Hassan J, Miyakita H, Reen DJ. Abnormal innervation and altered nerve growth factor messenger ribonucleic acid expression in ureteropelvic junction obstruction. J Urol. 1995;154:679–83.
154. Kuvel M, Canguven O, Murtazaoglu M, Albayrak S. Distribution of Cajal like cells and innervation in intrinsic ureteropelvic junction obstruction. Arch Ital Urol Androl. 2011;83:128–32.
155. Ozel SK, Emir H, Dervisoglu S, Akpolat N, Senel B, Kazez A, et al. The roles of extracellular matrix proteins, apoptosis and c-kit positive cells in the pathogenesis of ureteropelvic junction obstruction. J Pediatr Urol. 2010;6:125–9.
156. Koleda P, Apoznanski W, Wozniak Z, Rusiecki L, Szydelko T, Pilecki W, et al. Changes in interstitial cell of Cajal-like cells density in congenital ureteropelvic junction obstruction. Int Urol Nephrol. 2012;44:7–12.
157. Apoznanski W, Koleda P, Wozniak Z, Rusiecki L, Szydelko T, Kalka D, et al. The distribution of interstitial cells of Cajal in congenital ureteropelvic junction obstruction. Int Urol Nephrol. 2013;45:607–12.
158. Oliverio MI, Kim HS, Ito M, Le T, Audoly L, Best CF, et al. Reduced growth, abnormal kidney structure, and type 2 (AT2) angiotensin receptor-mediated blood pressure regulation in mice lacking both AT1A and AT1B receptors for angiotensin II. Proc Natl Acad Sci U S A. 1998;95:15496–501.
159. Burson JM, Aguilera G, Gross KW, Sigmund CD. Differential expression of angiotensin receptor 1A and 1B in mouse. Am J Phys. 1994;267:E260–7.
160. Miyazaki Y, Tsuchida S, Fogo A, Ichikawa I. The renal lesions that develop in neonatal mice during angiotensin inhibition mimic obstructive nephropathy. Kidney Int. 1999;55:1683–95.

161. Miyazaki Y, Tsuchida S, Nishimura H, Pope JC, Harris RC, McKanna JM, et al. Angiotensin induces the urinary peristaltic machinery during the perinatal period. J Clin Invest. 1998;102:1489–97.
162. Ismaili K, Hall M, Piepsz A, Alexander M, Schulman C, Avni FE. Insights into the pathogenesis and natural history of fetuses with renal pelvis dilatation. Eur Urol. 2005;48:207–14.
163. Travaglini F, Bartoletti R, Gacci M, Rizzo M. Pathophysiology of reno-ureteral colic. Urol Int. 2004;72(Suppl 1):20–3.